UNIVERSITY OF CALIFORNIA, SAN DIEGO

Characterization of the SLA domain in Zika Virus

A thesis submitted in partial satisfaction of the requirements
for the degree of Master of Science

in

Biology

by

Lourdes Carolina Myjak

Committee in Charge:

Professor Thomas C. Hermann, Chair
Professor Amy Pasquinelli, Co-Chair
Professor Nigel Crawford

2018

The Thesis of Lourdes Carolina Myjak is approved and it is acceptable in quality and form for publication on microfilm and electronically:

_____

_____

Co-Chair

_____

Chair

University of California, San Diego

2018

TABLE OF CONTENTS

LIST OF ABBREVIATIONS

AFM	Atomic Force Microscopy
CDC	Centers for Disease Control and Prevention
CS	Conserved Sequence
DENV	Dengue Virus
DNA	Deoxyribonucleic acid
eIF	Eukaryotic initiation factor
ER	Endoplasmic Reticulum
FRET	Fluorescence Resonance Energy Transfer
GFP	Green Fluorescent Proteins
HPLC	High-Performance Liquid Chromatography
IVT	*In vitro* transcription
NTP	Nucleotide triphosphate
Met-tRNA-i	Methionyl-initiator-tRNA
MM	Master mix
mRNA	Messenger RNA
Oligos	Oligonucleotides
ORF	Open reading frame
PABP	Poly(A) binding protein
PAGE	Polyacrylamide gel electrophoresis
PCR	Polymerase chain reaction
RdRp	RNA dependent RNA polymerase
RNA	Ribonucleic acid

RNAP	RNA polymerase
RT	Room temperature
SHAPE	Selective 2'Hydroxyl Acylation analyzed by Primer Extension
SLA	Stem Loop A
SLB	Stem Loop B
ssRNA	Single stranded RNA
TBE	Tris-borate-EDTA
TE	Tris-EDTA
tRNA	Transfer RNA
UAR	Upstream AUG Region
UTR	Untranslated region
UV	Ultraviolet

LIST OF FIGURES

LIST OF TABLES

ACKNOWLEDGEMENTS

I would like to thank Dr. Thomas Hermann for believing in me, allowing me to work in his lab and being a role model for me. He knew that I did not have enough research experience when I started out, but he gladly let me be part of his team. Without his help, support and patience I would not be the person that I am today.

I also would like to thank Dr. Amy Pasquinelli for being part of my thesis committee, and for making herself available for me.

I want to thank Dr. Nigel Crawford not only for being part of my committee, but for being a friend and a mentor.

Next, I would like to thank all the members of the Hermann lab including the ones that already left for all their friendship, encouragement, support and advice.

Lastly, I want to thank all my family and friends for all their support. Most importantly to my husband Robert Myjak, without him, I would not be where I am today. He has given me his unconditional support, has been very patient and has always been there to encourage me even when things seemed very difficult.

ABSTRACT OF THE THESIS

Characterization of the SLA domain in Zika Virus

by

Lourdes Carolina Myjak

Master of Science in Biology

University of California, San Diego, 2018

Professor Thomas C. Hermann, Chair
Professor Amy Pasquinelli Co-Chair

Phylogenetic analysis and sequence alignments with other Flaviviruses have led us to identify a putative promoter motif located in a putative three-way junction of the 5'UTR RNA, called Stem Loop A (SLA), which allows for binding of the RNA-dependent RNA polymerase (RdRp), and thus replication of the viral RNA genome. To support this hypothesis through structural and biochemical characterization of this domain, milligrams of the SLA RNA were

produced by *in vitro* transcription to then crystallize and determine its structure by X-ray diffraction. Determining the structure of the Zika virus SLA domain would contribute to our understanding of its mechanism of action. Although sufficient amounts of RNA were produced for crystallography, diffracting crystals have not yet been obtained. Additionally, a FRET assay has been developed and successfully used to confirm that the SLA domain of the Zika virus adopts a bent three-way junction conformation. FRET experiments with antisense DNA as surrogate ligands to parts of the SLA RNA suggest that the FRET assay will be useful in the future to discover small molecule ligands that alter and capture the SLA three-way junction in a non-functioning conformation.

INTRODUCTION

Flavivirus

Epidemic diseases were a big concern in the nineteenth century, mostly due to the lack of sanitation. In 1878 yellow fever posed a great threat in Memphis, Tennessee. [6] The disease caused fevers, chills, hemorrhaging, severe pains, and sometimes a jaundicing of the skin, which gave yellow fever its name [6,15]. It is believed that the disease was brought to the United States on slave ships from west Africa [6,15]. It was not until 1927 when the virus was isolated and confirmed that it was transmitted from person to person by the female *Aedes aegypti* mosquito [6]. Since yellowing of the skin was a hallmark symptom of infection with the virus it was named *Flavivirus* which is derived from the Latin "flavus" meaning "yellow".

Flaviviruses are enveloped positive\ single-stranded RNA viruses. Most of them are found in arthropods, primarily ticks and mosquitos, and can occasionally infect humans and other

animals. Mosquito transmitted *Flaviviruses* include Yellow fever, West Nile, Dengue, Japanese encephalitis and Zika. [31]

The virus enters the host cell and, once inside, the genomic RNA is released into the cytoplasm, where it serves as a mRNA. The mRNA takes over the host machinery to produce viral proteins. Host ribosomes on the endoplasmic reticulum (ER) initiate translation. The virus encodes three structural proteins (C, prM, E), and at least seven non-structural (NS) proteins. Production of new flaviviruses starts with the synthesis of a negative strand RNA by the RNA-dependent RNA polymerase (RdRp). The negative strand serves as a template for the positive strand genomic RNA which then associates to the capsid (C) by a yet unknown mechanism. The RNA-C complex buds into the ER where it acquires a lipid bilayer and viral proteins. After that, viral particles enter the Golgi apparatus which results in maturation and generation of new infective viraus. [12]

Dengue Virus (DENV)

As mentioned before, Dengue virus is a positive single stranded RNA virus of the family *Flaviviridae*. This virus has been studied extensively. Important elements were found in both the 5' and the 3' UTR's. The 5'UTR consist of a large Stem Loop A (SLA) that acts as a promoter in the synthesis of the circularized genome, a short stem loop B (SLB) which contains a 5' Upstream AUG Region (5'UAR) complementary to the 3' end of the viral genome (3'UAR), and a 5'Conserved Sequence (5' CS), both essential for long range RNA-RNA interactions [12] (**Figures 1-3**)

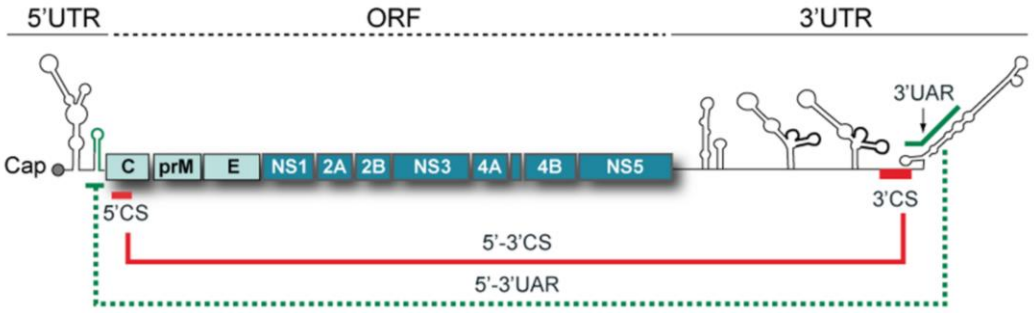

Figure 1. Dengue Virus RNA Genome [12]

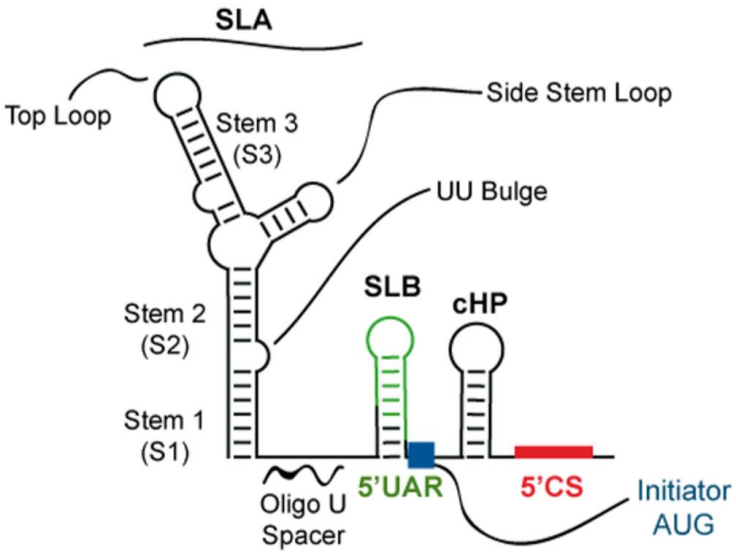

Figure 2. Dengue Virus 5' UTR RNA elements [12]

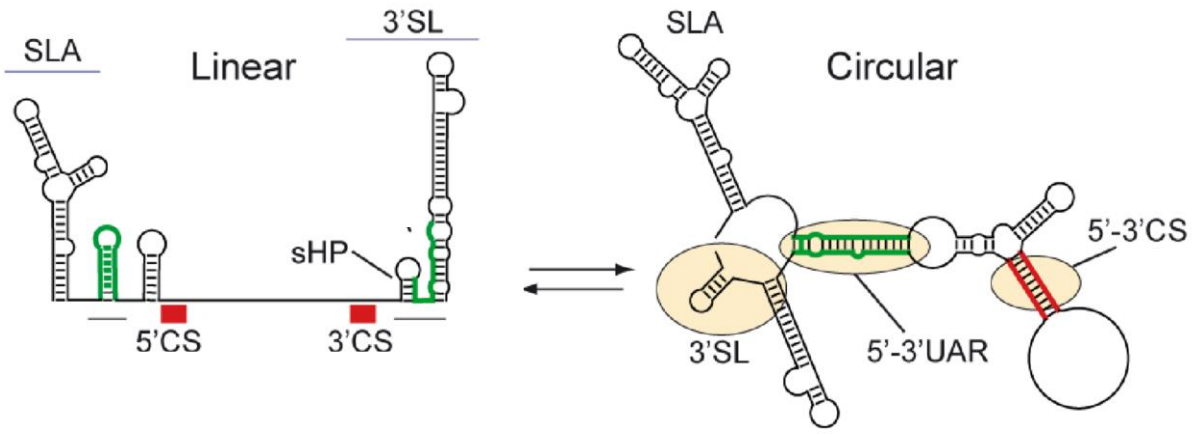

Figure 3. Cyclization of the DENV Cyclization requires at least two pairs of complementary regions 5'-3' CS and 5'-3' UAR [12]

Atomic Force Microscopy (AFM) demonstrated cyclization of individual molecules by long range RNA-RNA interaction [12]. Additionally, Selective 2'-Hydroxyl Acylation analyzed by Primer Extension (SHAPE), confirmed that the SLA forms a Y-shape structure and that some nucleotides are more reactive than others. These studies indicate the presence of three helical stems (S1, S2, and S3) adopting the fold of an RNA three-way junction [30].

Similar DENV SLA structures, 5'-3' CS and 5'-3' UAR were alsofound in other members of the *Flavivirus* genus [12].

Three-Way Junctions

Lescoute and Westhof, in their paper on "Topology of three-way junctions in folded RNAs" inspected published RNA crystal structures that had three-way junctions with the goal of finding sequence signatures that could be used for predicting the overall folding of the three-dimensional structure. They found that three-way junctions are necessary to promote long-range

RNA-RNA interactions. They also concluded that three-way junctions can be divided into three groups (or families) depending on the lengths of the junction strands, and that two of the helices are always found to be coaxially stacked as shown in the following figure:

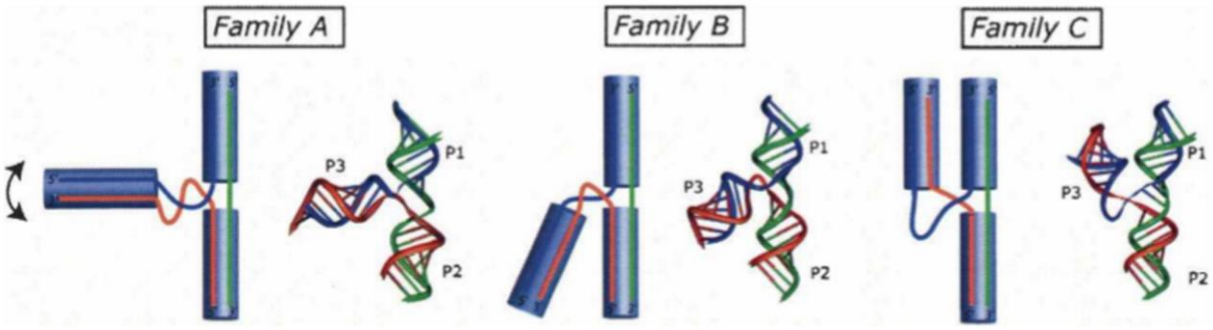

Figure 4. Schematic Drawings of the three observed families of RNA three-way junctions (A, B and C) [33]. The drawings are based on observations from RNA crystal structures. In family A the third helix can adopt various angles with respect to the coaxially stacked helices.

Zika Virus

The first cases of Zika exposure occurred in 1947 in Uganda, where monkeys were infected. Later, in the 1960 some human cases in Nigeria were observed. However, illness was not observed until an epidemic in the island of Yap in Micronesia which affected about 75% of the population infected with Ziika virus within a few months. In 2014 another epidemic was seen in French Polynesia (Tahiti), and in 2015 Zika infection was first seen in Brazil, after which it spread to Central America and then to the United States. It was then when the World Health Organization (WHO) declared Zika as a public health emergency of international concern in February 1, 2016 [36].

According to the Centers for Disease Control and Prevention (CDC), symptoms of Zika

infection can last for several days to a week, but once a person has been infected with the virus they are likely to be protected from future infections. While some of the most common symptoms associated with Zika are mild, including fever, rash, headache, joint pain, red eyes and muscle pain, infection by this virus can lead to serious conditions such as microcephaly.

Microcephaly is a condition where a baby's head is smaller in comparison to the average size. Microcephaly can occur when the baby's brain is not developed properly during pregnancy or has stopped growing after birth; this condition has the potential to be associated with other major birth defects. Depending on the severity, it can cause complications including seizures, developmental delay, intellectual disability, feeding problems, hearing and vision problems. These problems can range from mild to severe and are often lifelong afflictions. Unfortunately, there is no cure or standard treatment for this condition. [31, 36]

Zika virus is transmitted to people primarily through the bite of an infected *Aedes* species mosquito (*Ae. aegypti* and *Ae. albopictus*) [36]. It can also be transmitted through sex, needle sharing, blood transfusion, health care exposure and from mother to child (which leads to microcephaly). Moreover, another condition called Guillain-Barré syndrome has also been associated with Zika [36]. This is a condition that causes the immune system to attack a person's nerves, resulting in muscle weakness, tingling and even paralysis. [36]

As mentioned before, Zika is a positive single stranded RNA *flavivirus* (ssRNA) [16]. Phylogenetic studies have shown that Zika and Dengue Virus are closely related [19]. Combining information about conserved sequences in flaviviruses and three-way junctions, we predicted that the Zika virus contains two RNA domains within the 5' UTR with distinct functions during viral RNA synthesis. The first one is a large stem loop A (SLA), which has been proposed to act as a replication promoter in other flaviviruses such as DENV. The second domain is the short stem

loop B (SLB) containing the 5' upstream AUG region (5'UAR), which is complimentary to the 3' end of the viral genome (3'UAR) as shown in **Figure 5**.

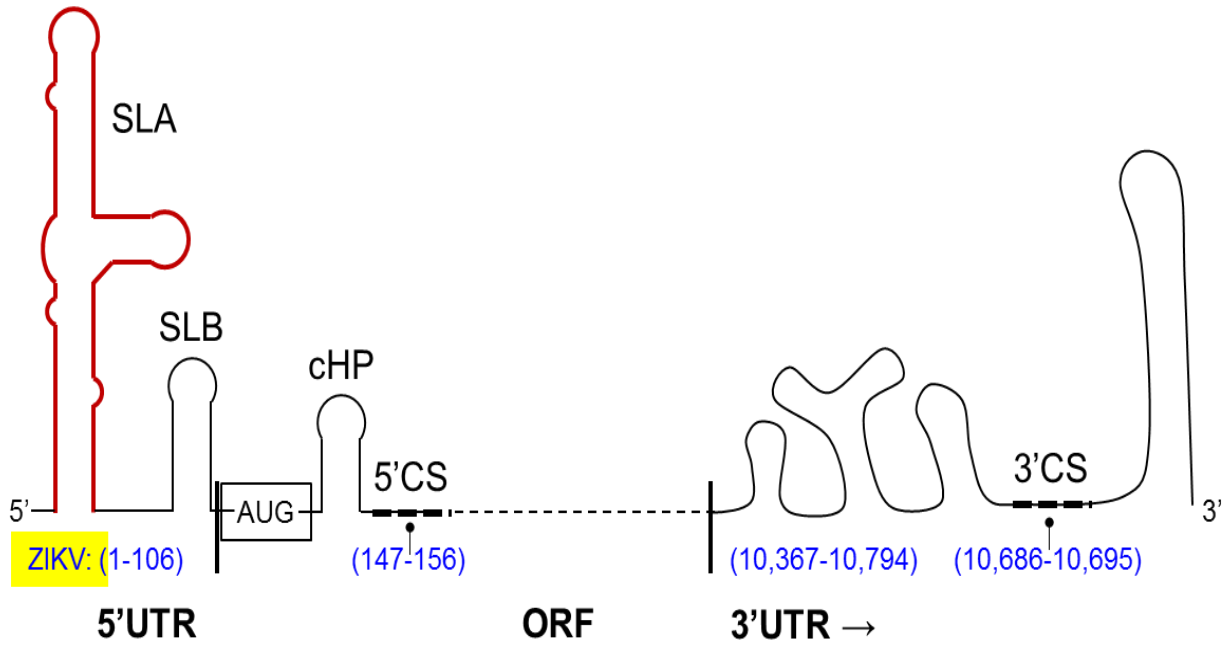

Figure 5. Predicted Domains of the Zika Virus Genome.

Studying the Zika SLA domain

In order for us to conclude whether the predicted SLA domain in Zika adopts a structure similar to the Dengue replication promoter, sufficient amounts of RNA are required. Since chemical custom synthesis of RNA containing over 30 nucleotides is expensive and often leads to impure product, we decided to prepare the ~ 70nt Zika SLA domain by *in vitro* transcription (IVT). There are three ways in which one can produce RNA by *in vitro* transcription [3] from different types of DNA templates, as shown in **Figure 6**.

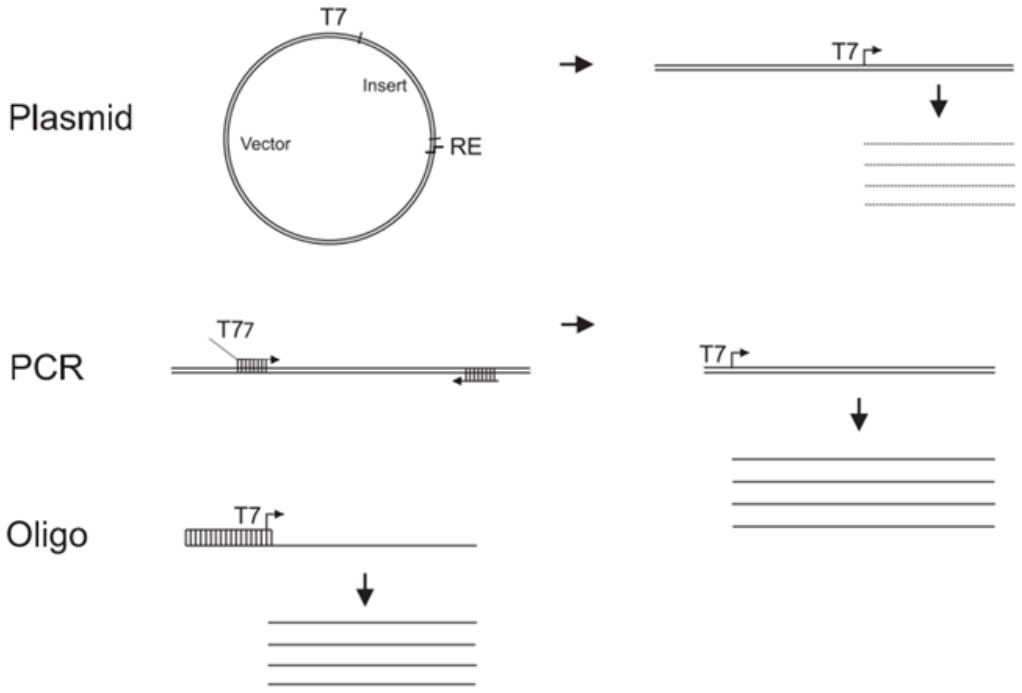

Figure 6. Synthesis of RNA by in vitro transcription [3]

I*n vitro* transcription requires a linear DNA template containing a double stranded promoter sequence for a bacteriophage RNA polymerase (SP6 or T7). This DNA template can be obtained from a linearized plasmid (preferred for sequences > 50 nt), a short PCR product sequence containing a SP6/T7 promoter sequence in the 5' end, followed by the sequence to be transcribed, and lastly, a synthetic DNA oligo containing the double-stranded SP6/T7 promoter sequence followed by the complementary sequence of interest.

The first six nucleotides after the promoter have a great impact in the production of RNA, and sequences starting with two guanosines produce the highest yields (**Figure 7**). Some high-yielding starting sequences are: GGGAGA, GGGAUC, GGCAAC, or GGCGCU [25].

Standard conditions for a 50 µL (small scale) transcription reaction include: 40 mM Tris-HCl buffer (pH 7.5), 40 mM dithiothreitol (DTT), 2 mM spermidine, 0.01% Triton-X 100 detergent, 5 mM nucleotide triphosphate (NTP), 10-50 mM $MgCl_2$ and 1.2 µM template or 5–10

μg linearized plasmid/ml transcription solution. Beginning from these standard conditions, the transcription is usually optimized by changing the concenration of Mg^{2+}, NTPs, template DNA, RNA polymerase and the time of transcription [11].

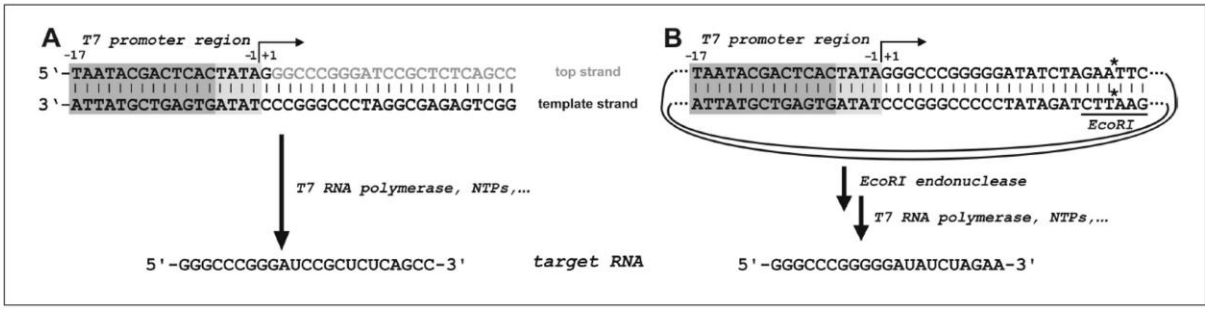

Figure 7. T7 promoter sequence. Transcription of RNA with indication of the +1 nucleotides where G corresponds to the 1st nucleotide in transcript [11]

Like DNA polymerases, RNA polymerases have a tendency for premature termination or addition of non-encoded nucleotides at the 3' end of the synthesized strand, leading to heterogeneous 3' ends or run-off transcripts. To overcome this to obtain homogenous transcripts, ribozyme sequences can be added on the 5' and/or the 3' end of the desired RNA sequence. Ribozymes will then cleave at their corresponding sequence. Some of the most used ribozymes include the hammerhead and hairpin ribozymes which require specific upstream sequences. The hepatitis delta virus (HDV) overcomes this drawback with a catalytic RNA domain that has no requirement for the sequence upstream of the cleavage position, making it useful for the preparation of homogenous 3' ends without affecting the sequence of the transcribed RNA product of interest [25]. The transcription time varies between 2–4 h and is usually shortened as the RNA sequence increases to avoid degradation of longer products. Even though synthetic DNA can be used, a cloned plasmid provides an unlimited source of template DNA with fewer chances of mutations than in PCR products.

RNA purification and crystallization

Transcription of RNA usually yields more than one product due to premature termination or addition of additional nucleotides. Therefore, RNA purification is a critical step [34], especially for crystallization purposes. The required degree of purification after the transcription reaction depends on what will be done with the RNA transcripts [13]. Phenol chloroform extraction, for example, followed by alcohol precipitation will remove all enzymes and free nucleotides. Another purifying method is High-Performance Liquid Chromatography (HPLC) which separates the different components in a mixture. Yet, the most common and efficient method of purifying RNA is by preparative denaturing Polyacrylamide Gel Electrophoresis (PAGE). PAGE gels can separate the sequence of interest from short single nucleotides or fractionation of the desired product [25] as shown in **Figure 8**.

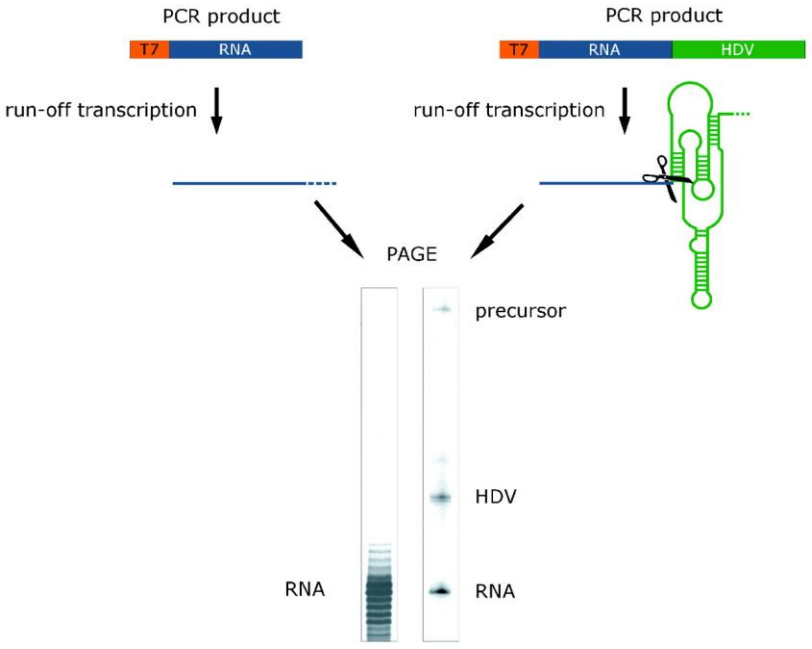

Figure 8. PAGE fractionation of PCR. Example of a fractionation of RNA [25]

Determining the location of the RNA band of interest is critical because this band can be cut out and eluted out of the gel by UV shadowing and then precipitated for further use

FRET

Fluorescence Resonance Energy Transfer (FRET) or Förster Resonance Energy Transfer is an assay involving two fluorophores , a “donor” and an “acceptor” dye, where the donor fluorophore is excited at a particular wavelength and the energy released is transferred to the acceptor fluorophore without emission of a photon. If the FRET donor and acceptor pair is close enough then fluorescent light is emitted from the acceptor [22, 23] as shown in **Figure 9**

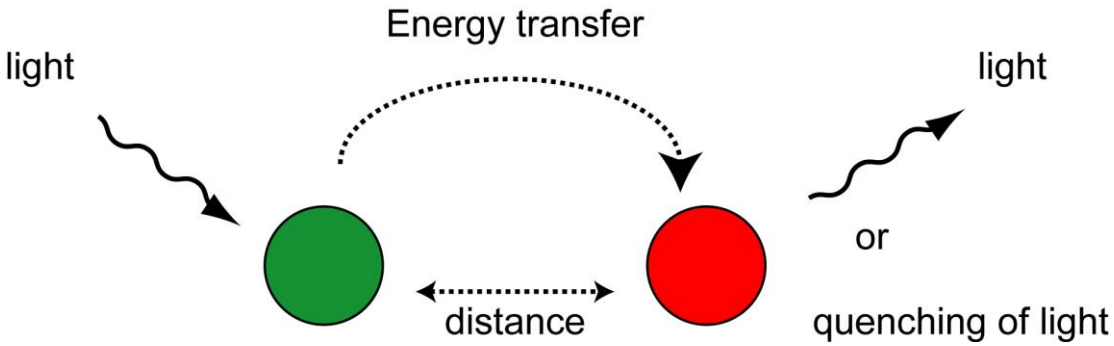

Figure 9. FRET assay principle [26]. This figure shows that if the donor molecule is excited and the acceptor molecule is close enough, there will be energy transfer that will be emitted by the acceptor molecule as light.

The efficiency of FRET is dependent on the inverse sixth power of separation between donor and acceptor dye, making FRET a sensitive technique for investigating a variety of biological phenomena that produce changes in molecular proximity (such as molecule

conformation or molecule binding interactions) [23,26,27]. Nevertheless, certain requirements must be met; for example, donor and acceptor molecules must be within a distance of 10-100 Å; and the absorption spectrum of the acceptor dye must overlap the fluorescence emission spectrum of the donor dye [9,22] as shown in **Figure 10.**

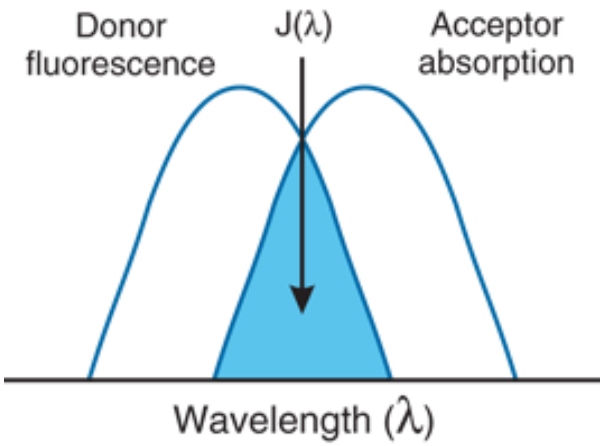

Figure 10. Overlap of the emission spectrum. Overlap of the emission spectrum of donor and acceptor dyes.

The organic cyanine dyes Cy3 Cy5 , Cy5.5 and Cy7 emit in the red range (greater than 550 nm) which is a desirable range because near-infrared emissions of light are usually more sensitive and have less interference by other sources. Cy3 emits maximally at 570 nm and Cy5 emits at 670 nm with a Förster distance greater than 50 Å [26].

The FRET method would provide valuable information in our investigation. If we are correct in assuming that DENV and ZIKV are very similar. Then ZIKV's SLA domain will also adopt a flexible three-way junction conformation. This hypothesis can be investigated by using the FRET assay; for example, the FREt experiment can provide information as to which of the helices in the three-way junction are coaxially stacked. Additionally, this assay can be used to measure the effect of ligand binding on the FRET signal.

Aims

For functional studies, we used the FRET assay. Our first aim was to create a construct where we could confirm that the SLA domain is a three-way junction and to determine which helical parts of this domain are coaxially stacked. The second aim was to investigate interaction of the SLA domain with small molecules in the same assay while observing the effect of the addition of those molecules on the FRET signal.

Furthermore, the three-dimensional structure of the SLA domain in Zika virus would offer valuable insight into the structural basis of function of the replication promoter. To determine the structure of the RNA domain, the first aim was to generate DNA templates that could be used for *in vitro* transcription of the SLA domain. The second aim was to optimize *in vitro* transcription to produce larger amounts of RNA for crystallography, and lastly, to obtain diffracting crystals.

RESULTS

FRET

We started by doing a sequence alignment between DENV SLA domain and ZIKV predicted SLA domain. We confirmed that there were conserved motives between the two viral seuences. From there, two constructs, ZRP1 and ZRP2, containing fluorophores Cy3 and Cy5 respectively were designed to model the Zika virus SLA as shown in **Figure 11**. These two sequences form the backbone that make up the SLA domain; they are expected to anneal by Watson-Crick base pairing and fold toproduce a FRET signal under proper excitation conditions. This domain has three helical domain components P1, P2 and P3 as shown on **Figure 12**. The ZRPAx constructs (x being number of nucleotides) are antisense DNA strands of varying lengths (**Table 1**) that are expected to bind and destabilize the P3 arm of the ZRP1/ZRP2 complex and thereby alter the FRET signal. Here, the amounts of ZRPx were varied by 0, 1, 2, 4, and 8 fold higher relative to ZRP1/2 concentration. Additionally, various concentrations of promiscuously RNA-binding aminoglycoside antibiotics on the ZRP1/2 complex were tested. The antibiotics that we used included neomycin, paromomycin, and tobramycin because they are known to bind to structured RNA molecules. We wanted to explore if the aminoglycoside antibiotics would bind to the ZRP1/2 complex and cause a conformational change that may block the SLA domain and thus inhibit viral replication.

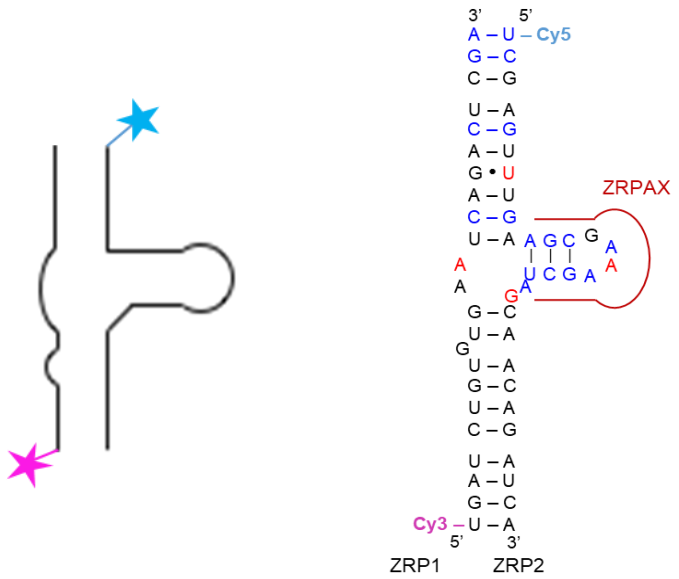

Figure 11. FRET construct design. ZRP1 and 2 are predicted to form a complex. ZRP1 carries a Cy3 dye and ZRP2 is conjugated with a Cy5 dye. Antisense DNA ZRPAx will bind to the ZRP2 to destabilize the three-way junction.

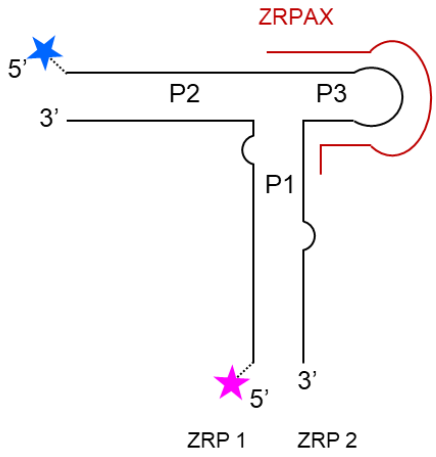

Figure 12. Predicted SLA domain as a conformationally flexible three-way junction. Predicted SLA secondary structure with 3 helical components P1, P2 and P3 in which DNA antisense oligos Ax will bind the ZRP2 at the hairpin loop P3.

Table 1. Oligo names and sequences. ZRP1/2 is predicted to form a complex and are the only two oligos with fluorophores. ZRPA will bind to ZRP2 and will destabilize the P3 arm. ZRPC is a scrambled control sequence.

Name	Sequence
ZRP 1:	5’ Cy3-UGA UCU GUG UGA AUC AGA CUC GA
ZRP 2:	5’ Cy5-UCG AGU UUG AAG CGA AAG CUA GCA ACA GAU CA
A-12	5’ CT AGC TTT CGC T
A-15	5’ T GCT AGC TTT CGC TT
A-20	5’ GTT GCT AGC TTT CGC TTC AA
A-26	5’ TCT GTT GCT AGC TTT CGC TTC AAA CT
A-32	5’ TGA TCT GTT GCT AGC TTT CGC TTC AAA CTC GA
ZRPC:	5’ GTT CGT TGC TTA TCC *

To test our hypothesis whether or not the SLA domain in ZIKV is a three-way junction and to create a robust-FRET based assay, we first started by testing the impact of different Mg^{2+} concentrations and different annealing protocols on RNA folding. We were expecting that as the Mg^{2+} concentration increased, the complex will form and if we are correct to assume that one of the arms adopts different angles (similar to the family A of three-way junctions) then we will see an increase in FRET due to folding of the RNA.

In the first experiment the protocol used was 65SNAP5 (samples were heated at 65 °C for 5 minutes then snap cooled at 4 °C for another 5 min) and the results were the following:

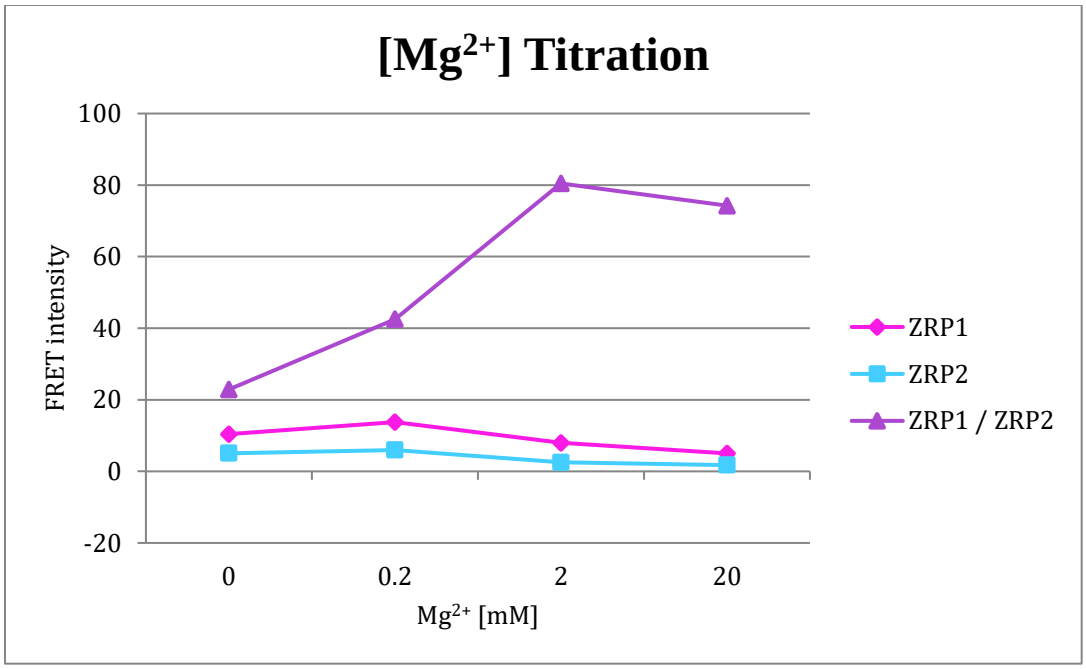

Figure 13. Mg^{2+} Titration. This graph shows that 2 mM Mg^{2+} was the point at which the highest FRET signal was recorded. Additionally, we observed that a FRET signal ocured only with the ZRP1/2 compelx but not with the individual oligos. The concentration of ZRP1-2 strands were 0.1 µM and the Mg^{2+} concentration was 0, 0.2, 2, and 20 mM.

This experiment confirmed our hypothesis that the SLA domain in ZIKV adopts a three-way junction fold in which helical regions P2 and P3 are coaxially stacked and 2 mM Mg^{2+} are required for folding of the construct.

Although the results confirmed our hypothesis on the three-way junction fold of the SLA RNA, a higher FRET signal with a higher signal-to-noise ratio was desired for the future screening of ligand binding. We tested different annealing protocols such as: 37 °C for 30 min followed by a 10 min incubation at room temperature (RT) with the same Mg^{2+} concentrations (37C30 → 10RT); 65 °C for 5 min, 4 °C for 5 min, 37 °C for 30 min and 10 min at RT with the same Mg^{2+} concentrations (65SNAP5, 37C30 → 10RT). Among these protocols, the last one gave the best results.

Afterwards, we wanted to test our second hypothesis. If we are correct in assuming that the conformation of the SLA domain can be affected by small molecule liagnds, then destabilization of the P3 helical arm by antisense DNA will cause a conformational change. We predicted that a short DNA would not cause a conformational change due to its inability to form a stable complex with the RNA target; a long DNA oligo would bind to the ZRP2 component and cause dissociation of the construct, thereby quenching the FRET signal, but a DNA of the right length would associate with the RNA target in a ternary complex and cause a conformational change reported by a change in the FRET signal. If this is true then we can use the SLA FRET construct in an assay to test small molecules for binding to this viral RNA domain.

To see the effect of the DNA oligo length on binding with the ZRP1/2 complex, we annealed the construct with 2 mM Mg^{2+} and DNA oligos of different lengths, leading to the following observations:

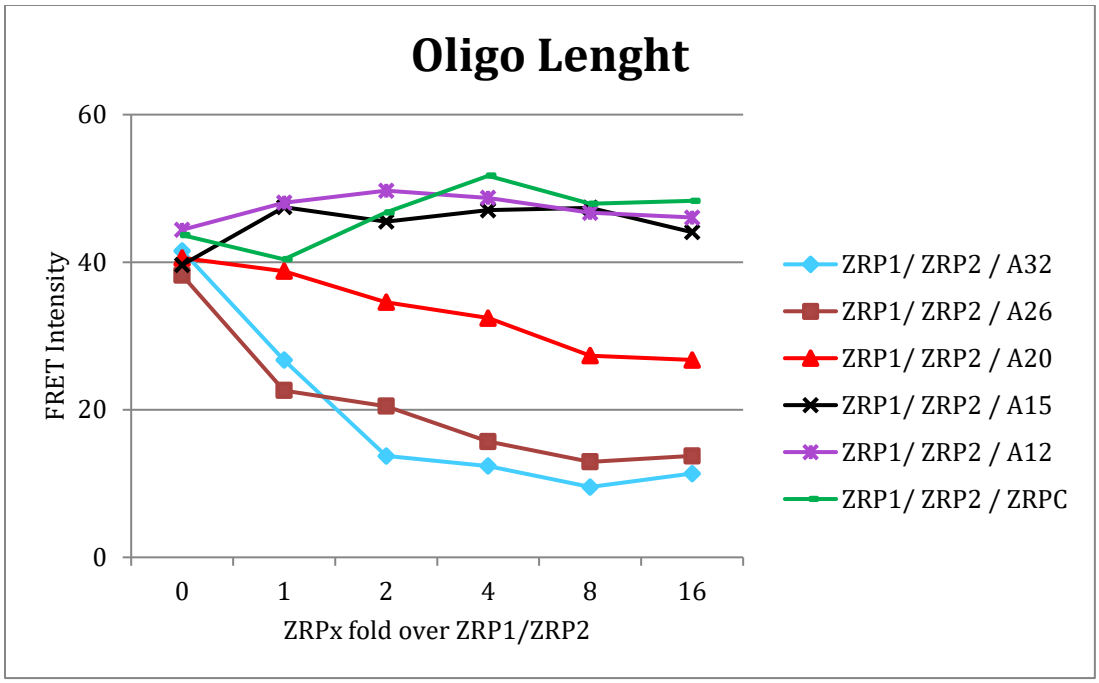

Figure 14. Effect of oligo length on DNA antisense binding to the ZRP1/2 complex. Antisense oligos A12 (12nt length) to A32 (32nt length) were tested.We observed that DNA oligos A26 and 32 dissociated the complex leading to strongly reduced FRET signal. DNA A12, A15 and the scrambled control ZRPC did not cause a dissociation of the complex, and no change in signal was observed. DNA A20 did decrease but not abolish the FRET signal, suggesting that an alternative conformation was captured in a ternary complex. This experiment was performed at 65SNAP5, 37C30 → 10RT with [Mg^{2+}] of 2 mM. ZRP1/2 both at 0.1 µM and the oligo concentration was 0, 1,2, 4, 8 and 16 times more with respect to ZRP1/2, (1, 0.1, 0.2, 0.4, 0.8 and 1.6 µM respectively).

This experiment confirmed our hypothesis, that the conformation of ZIKV SLA domain can be captured through ligand binding to the three-way junction. Subsequently, we tested the RNA binders neomycin, paromomycin and tobramycin in comparison with DNA oligos A15, A20 and A26 as controls and determined the effect of these antibiotics on our construct. The results of this experiment are the following:

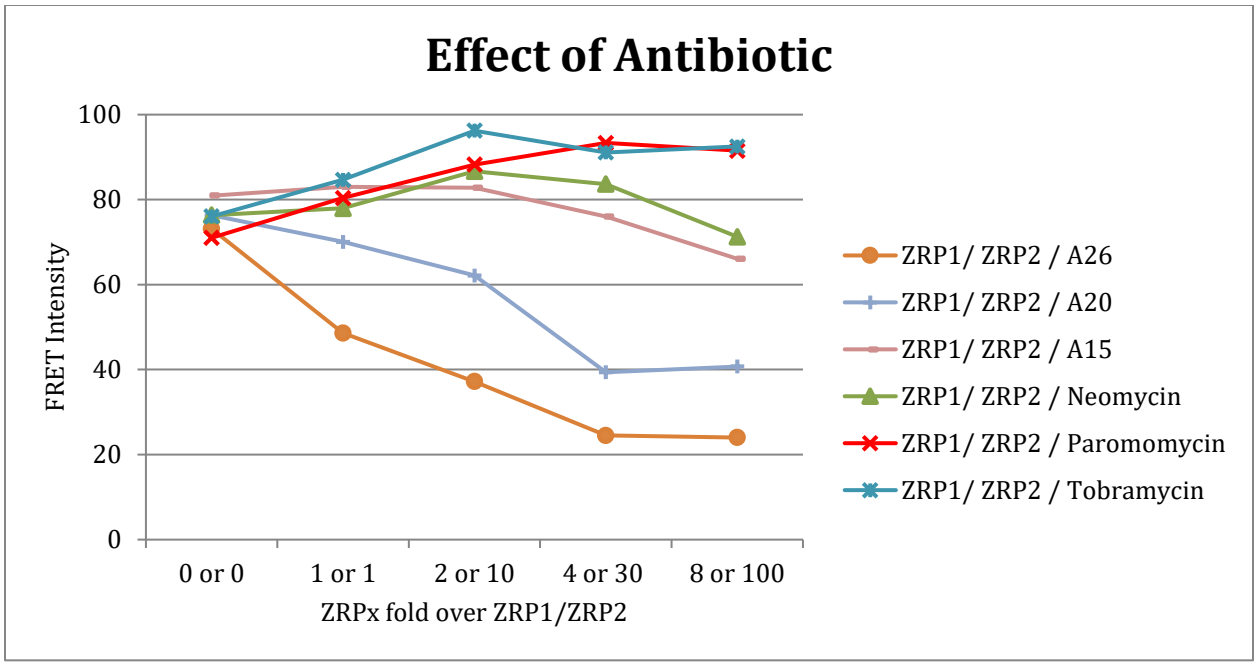

Figure 15. Effect of RNA-binding antibiotics. Here we saw that A15 did not change FRET signal, A 26 dissociated the construct and A20 had some effect in our assay, as previously observed. Additionally, the antibiotics behaved in as similar ways as the small DNA oligo and did not affect the FRET signal. The protocol used was 65snap5 37C30 → 10RT with [Mg^{2+}] of 2 mM. ZRP1/2 both at 0.1 µM and the oligo concentration were: 0, 0.1, 0.2, 0.4, and 0.8 µM. The antibiotic concentration was 0, 1, 10, 30 and 100 µM.

Here, we observed that the addition of antibiotics did not affect the FRET signal, suggesting that the compound do not bind or alter the conformation of the RNA target.

The next experiments varied the antibiotic concentration, and additionally we tested urea, formamide and guanidine (results not shown) which act as denaturants and perturb hydrogen bonding; the results were similar. Since we were expecting a decrease in FRET because of the breaking of H bonds, but saw no significant difference, we decided to step back, and optimize our constructs and determine which annealing protocol wilwouldl consistently give us higher signal whether we use an antisense DNA surrogate ligand or not.

Table 2. Comparison of annealing protocols. This table indicates the different protocols that were tested to compare the FRET signal when the added oligo was annealed with the ZRP1/2 complex or added to the complex after the annealing.

Protocols

	RT			65SNAP5			65SNAP5 → 37C30			MM → 65SNAP5 → PX		
	1	**2**	**3**	**4**	**5**	**6**	**7**	**8**	**9**	**10**	**11**	**12**
A	24 µL MM 96 µL buffer			24 µL MM 96 µL buffer 65SNAP5			24 µL MM 96 µL buffer 65SNAP5 → 37C30					
B	24 µL MM 24 µL PX 72 µL buffer			24 µL MM 24 µL PX 72 µL buffer 65SNAP5			24 µL MM 72 µL buffer 65SNAP5 34 µL PX → 37C30			24 µL MM 72 µL buffer 65SNAP5 → 24 µL PX		

Protocols

MM (master mix): ZRP1 + ZRP2 + Mg^{2+}

ZRP1 / ZRP2

1. Make MM + buffer at RT and read

2. Make MM + buffer 65SNAP5 and read

3. Make MM + buffer 65SNAP5 then 37C30 read

ZRP1 / ZRP2 / ZRPA2

1A. Make MM add PX and buffer at RT and read

2A. Make MM + buffer 65SNAP5 add PX and read

3A. Make MM + buffer 65SNAP5 add PX 37C30 and read

4A. Make MM + buffer + PX 65SNAP5 and read

These results suggested that temperature played an important role in the RNA annealing process and may explain the only minimal changes in FRET when the antibiotics were added. Additionally, three different SLA RNA constructs were designed, including longer constructs to increase the dynamic range for FRET and a mutant that will lock the three-way junction as shown in **Table 3 and Figure 16.**

Table 3. Modified RNA constructs. Modified RNA constructs: ZRP1- m1 is a mutant version of ZRP1. ZRP1-4 and ZRP2-4 indicate that 4 additional nucleotides were added to the original ZRP1/2 constructs.

RNA constructs		
ZRP 1-m1	5'	Cy3-UGA UCU GUG UGC UC AGA CUC GA
ZRP 1-4	5'	Cy3-UG CG A UCU GUG UGA AUC AGA CU AG C GA
ZRP 2-4	5'	Cy5-UCG CU AGU UUG AAG CGA AAG CUA GCA ACA GAU CG CA

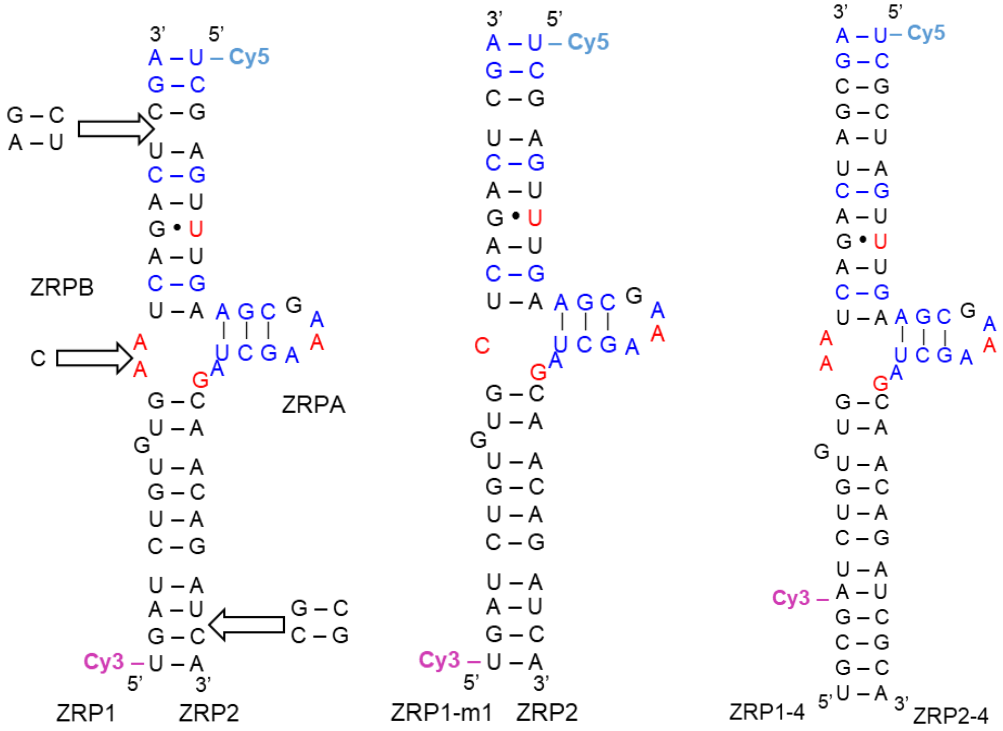

Figure 16. Modified ZIKV SLA RNA constructs.

In order to obtain more consistent data and to control the temperature factor, we created a program in which the oligos were heated at 65 °C for 5 min, cooled down at 4 °C for 5 minutes (similar to our 65SNAP5); however, we added an incubation of 37 °C for 10 min followed by a minimum of 2 min at RT (22 °C). This protocol was labeled as 65SNAP20

Eventually, the FRET constructs and protocols were transferred in a collaboration with another graduate student in the lab for further FRET experiments while I tfocused on investigating the interaction of the SLA RNA constructs with different antisense DNA oligos by native polyacrylamide gel electrophoresis (PAGE). To achieve this, 13% native polyacrylamide gels were used; to simplify the labels, ZRP1 was labeled as short 1 (s1) ZRP2 (s2), ZRP1-4 was labeled Long (L1) and ZRP2-4 (L2). The results are the following:

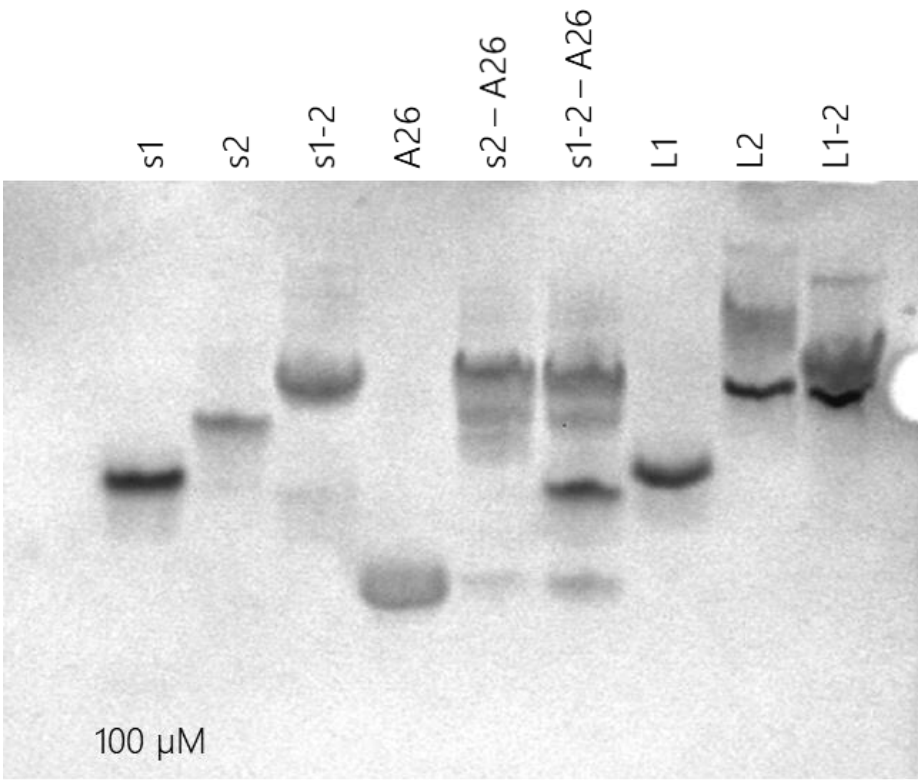

Figure 17. Native PAGE of ZRP1/2 vs ZRP 1-4/2-4. Comparing the small complex with the large complex plus confirming the destabilization of the P3 arm by the addition of antisense DNA oligo A26. The conditions of the gel were: Native gel (13% Polyacrylamide, 2X MOPS, 10% APS, 2mM Mg^{2+}, TEMED), Loading Buffer (2mM Mg^{2+}, 50 % glycerol, 4X MOPS), Running Buffer (2X MOPS, 2mM Mg^{2+}, H_2O) Reaction Buffer (3 µL/sample: 20mM HEPES pH 7.0, 2mM Mg^{2+}, Sample RNA and A2 at 100uM concentration and using 65SNAP5 annealing protocol) 4 µL sample was added and run at 220 V

The gel shows that ZRP1/2 in fact do form a complex. Additionally, the gel shows some non-stable binding of ZRP2 with A26. Additionally, when all three oligos are combined a band corresponding to the formation of the ternary structure is absent. These results agree with what we observed in our FRET experiments. Our next step was to determine which DNA oligos had the "right" size to form a complex without dissociating the SLA construct. To do that, we tested antisense DNA oligos of different lengths by native PAGE, and here are the results:

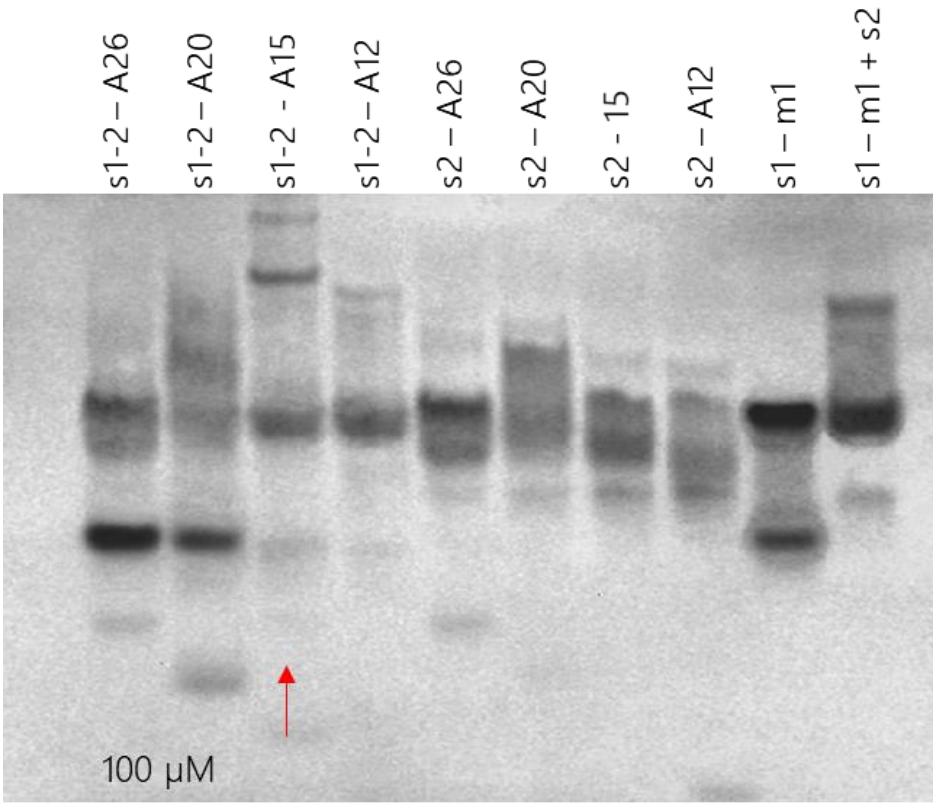

Figure 18. Most suitable antisense DNA oligo. This gel demonstrated that only oligo A15 was the one forming the ternary complex. All other DNA oligos were not stable as seen by the smears. ZRP1-m1 was also not stable. The conditions of the gel were: Native Gel (13% Polyacrylamide, 2X MOPS, 10% APS, 2mM Mg^{2+}, TEMED), Loading Buffer (2mM Mg^{2+}, 50 % glycerol, 4X MOPS), Running Buffer (2X MOPS, 2mM Mg^{2+}, H_2O) Reaction Buffer (3 µL/sample: 20mM HEPES pH 7.0, 2mM Mg^{2+}, Sample RNA and Ax at 100uM concentration using 65SNAP5 annealing protocol) 4 µL sample was added and run at 220 V

As shown on the previous figure, only the DNA oligo A15 was the one forming a ternary complex with ZRP1/2. After that, we wanted to test the longer SLA RNA construct with oligo A15 at different concentrations (0, 1, 2, 4, and 8-fold the concentration of the RNA) to see if we also saw the complex. The results are the following:

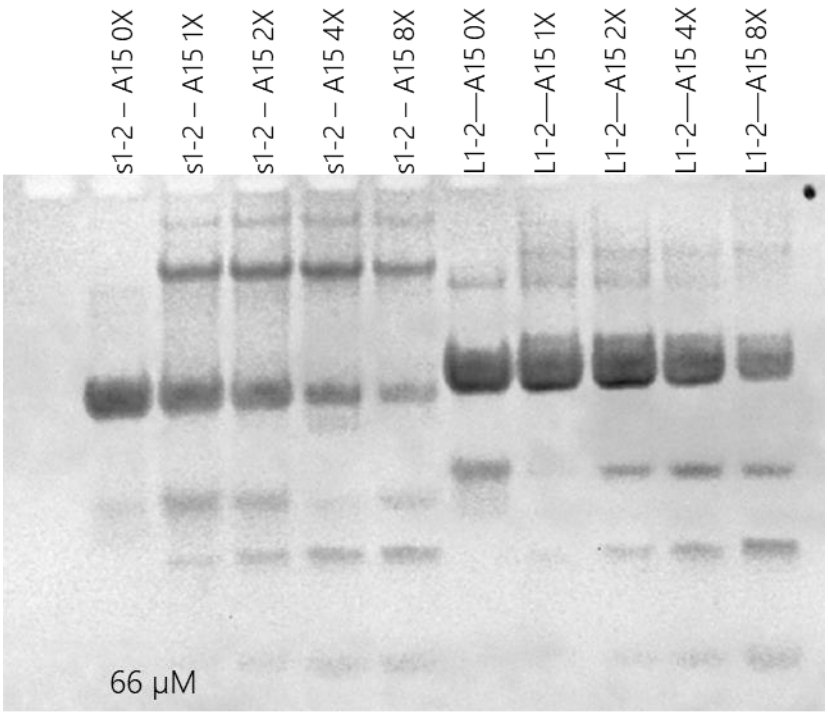

Figure 19. Effect of short and long SLA constructs with oligo A15. Since A15 was the only one forming the complex with the small construct, we tested A15 with the longer constructs. We confirmed again that the short construct was indeed forming a complex, however, we did not see any bands for the large complex. The conditions of the gel were: Native Gel (13% Polyacrylamide, 2X MOPS, 10% APS, 2mM Mg^{2+}, TEMED), Loading Buffer (2mM Mg^{2+}, 50 % glycerol, 4X MOPS), Running Buffer (2X MOPS, 2mM Mg^{2+}, H_2O) Reaction Buffer (3 µL/sample: 20mM HEPES pH 7.0, 2mM Mg^{2+}, Sample RNA at [66uM] and A at [0, 66, 132, 264, 528 µM] using 65SNAP5 annealing protocol) 4 µL sample was added and run at 220 V

Here, we confirmed again that A15 was forming a complex with ZRP1/2 (the short construct). However, A15 did not form a complex with the longer SLA construct. Some faint bands indicated a ternary complex, but the yield was very low. We were expecting much sharper bands. Therefore, we decided to test the A26 oligo. The results were as follow:

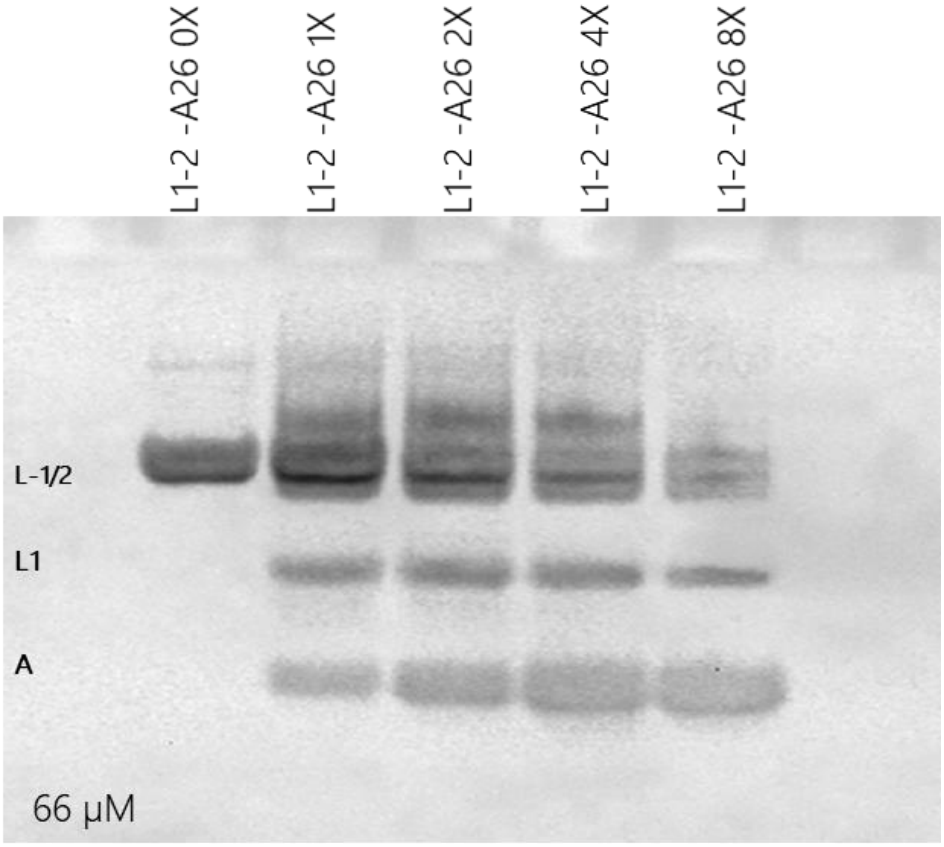

Figure 20. ZRP1-4/2-4/A2 complex. The second band is ZRP1-4 by itself and the one at the bottom was A26. The conditions of the gel were: Native Gel (13% Polyacrylamide, 2X MOPS, 10% APS, 2mM Mg^{2+}, TEMED), Loading Buffer (2mM Mg^{2+}, 50 % glycerol, 4X MOPS), Running Buffer (2X MOPS, 2mM Mg^{2+}, H_2O) Reaction Buffer (3 µL/sample: 20mM HEPES pH 7.0, 2mM Mg^{2+}, Sample RNA at [66uM] and A2 at [0, 66, 132, 264, 528 µM] using 65SNAP5 annealing protocol) 4 µL sample was added and run at 220 V

In **Figure 20,** we only had smears, therefore we had to test all the different antisense DNA oligos to determine which one forms a ternary complex. Additionally, we wanted to make comparisons between the shorter and the larger SLA constructs. The results are the following:

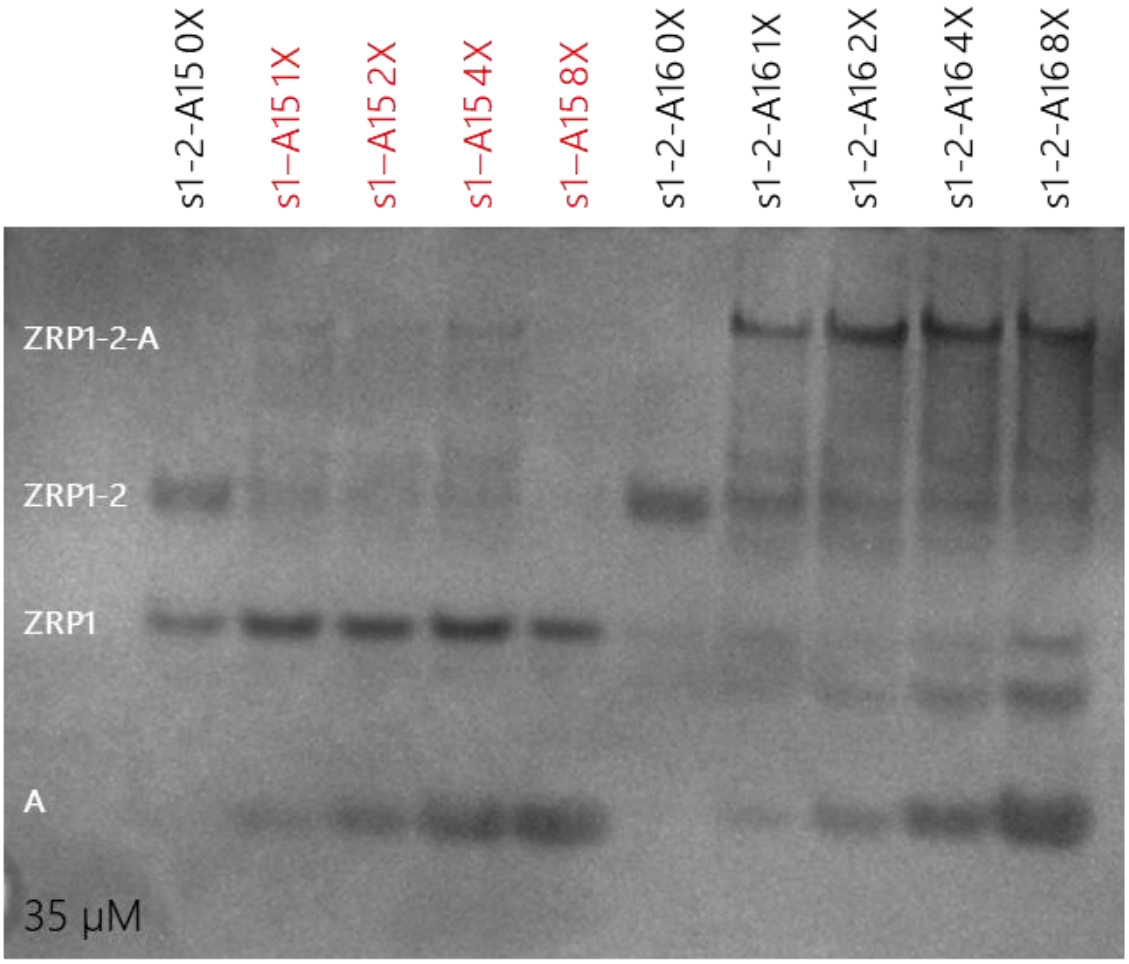

Figure 21. ZRP1/2 + A15/A16. This gel indicates that both A15 and A16 DNA were forming a ternary complex. The lanes labeled in red indicate that only ZRP1 was added inadvertently. The conditions of the gel were: Native Gel (13% Polyacrylamide, 2X MOPS, 10% APS, 2mM Mg^{2+}, TEMED), Loading Buffer (2mM Mg^{2+}, 50 % glycerol, 4X MOPS), Running Buffer (2X MOPS, 2mM Mg^{2+}, H_2O) Reaction Buffer (3 µL/sample: 20mM HEPES pH 7.0, 2mM Mg^{2+}, Sample RNA at [35 µM] and Ax at [0, 35, 70, 140, 280 µM] using 65SNAP5 annealing protocol) 4 µL sample was added and run at 220 V

In **Figure 21,** we observed that a complex was forming with the A16 DNA and the shorter SLA construct. Although there are not results for A15, this oligo was tested twice previously and both times it formed the complex.

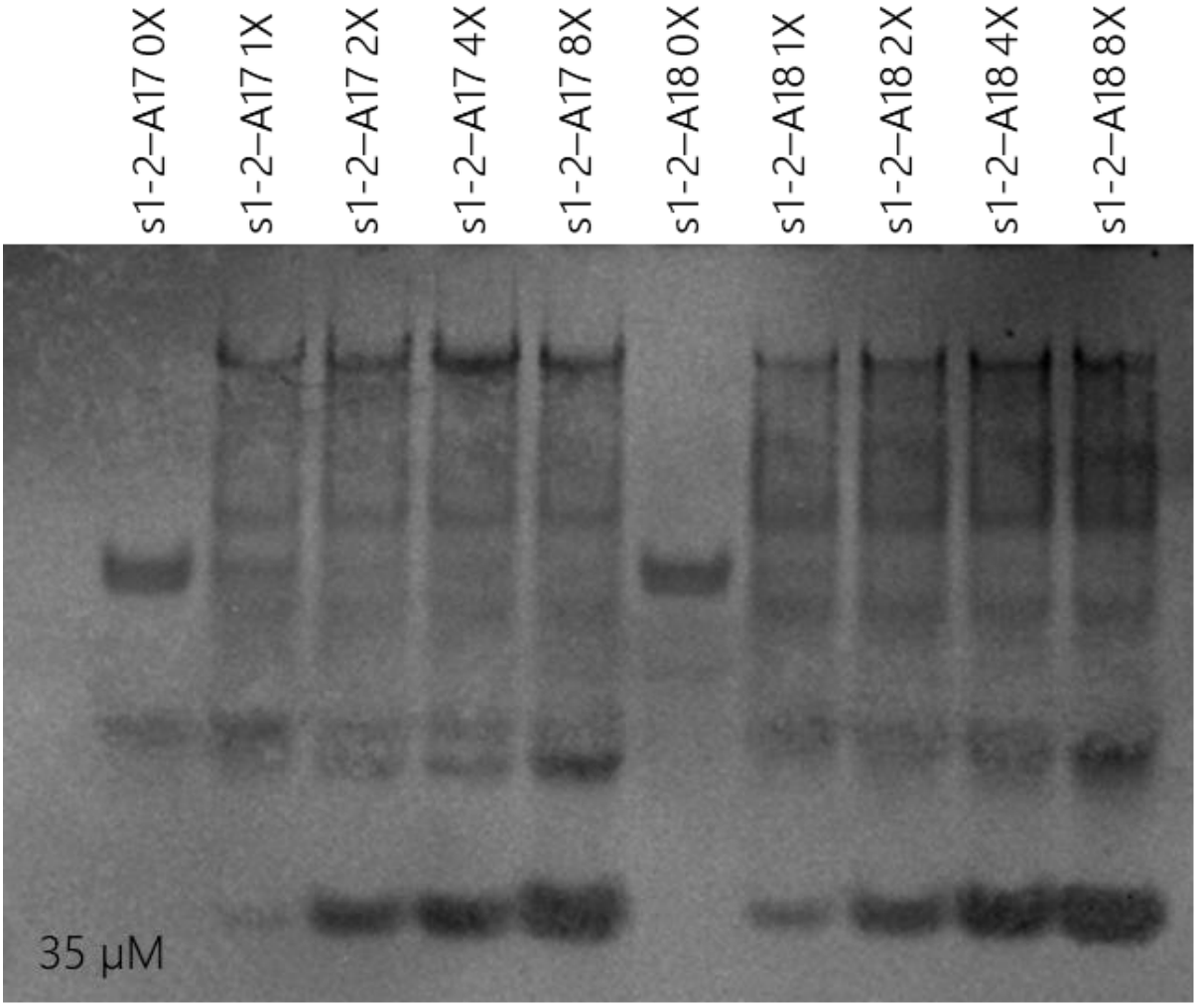

Figure 22. ZRP1/2 +A17/A18. Here we see that the complex is forming again. However, the band for complex using A18 is not as dark. The conditions of the gel were: Native Gel (13% Polyacrylamide, 2X MOPS, 10% APS, 2mM Mg^{2+}, TEMED), Loading Buffer (2mM Mg^{2+}, 50 % glycerol, 4X MOPS), Running Buffer (2X MOPS, 2mM Mg^{2+}, H_2O) Reaction Buffer (3 µL/sample: 20mM HEPES pH 7.0, 2mM Mg^{2+}, Sample RNA at [35 µM] and Ax at [0, 35, 70, 140, 280 µM] using 65SNAP5 annealing protocol) 4 µL sample was added and run at 220 V

In **Figure 22.** The complex is formed using A17 DNA; however, using A18 DNA, the bands for the complex are not as dark suggesting perhaps that this represents the length at which the DNA oligos are starting to cause dissociation of the ZRP1/2 SLA complex.

The results from the longer constructs ZRP1-4/2-4 + Ax are the following:

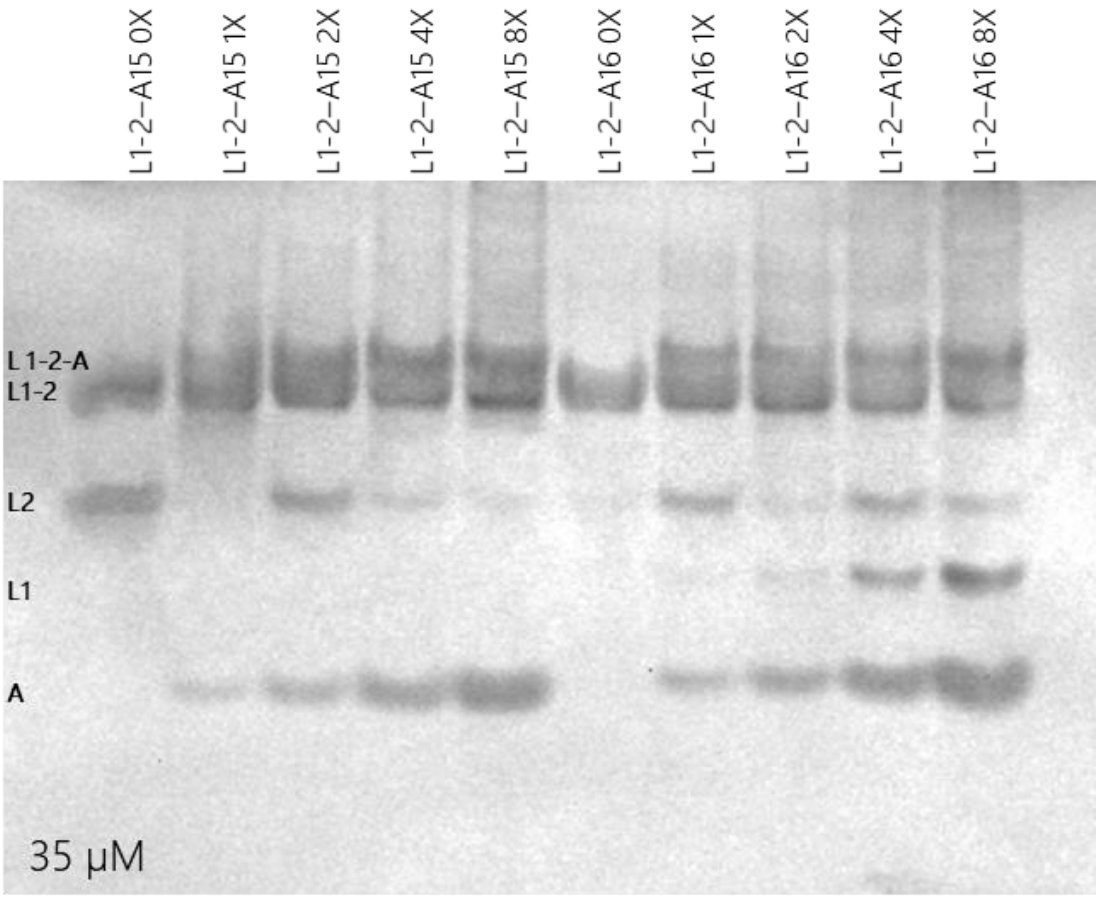

Figure 23. ZRP1-4/2-4 + A15/A16. Here we do not see any complex because the gel shows a smear bands, indicating again that the ternary complex is not stable. The conditions of the gel were: Native Gel (13% Polyacrylamide, 2X MOPS, 10% APS, 2mM Mg^{2+}, TEMED), Loading Buffer (2mM Mg^{2+}, 50 % glycerol, 4X MOPS), Running Buffer (2X MOPS, 2mM Mg^{2+}, H_2O) Reaction Buffer (3 µL/sample: 20mM HEPES pH 7.0, 2mM Mg^{2+}, Sample RNA at [35 µM] and Ax at [0, 35, 70, 140, 280 µM] using 65SNAP5 annealing protocol) 4 µL sample was added run at 220 V

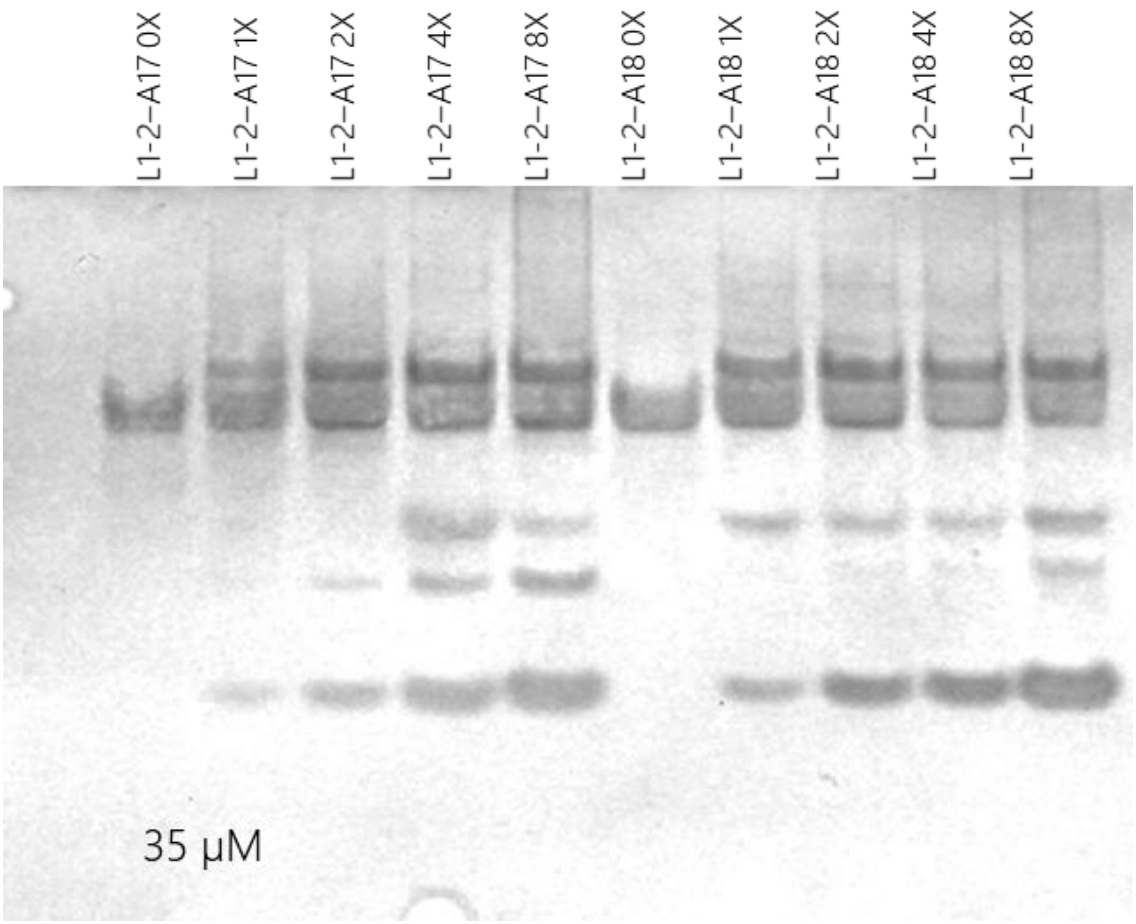

Figure 24. ZRP1-4/2-4 + A17/A18. Here we are starting to see some separation between the longer construct (only L1-2 bound) and the longer complex (L1-2-Ax). Additionally, it seems that both complexes form in equal proportions. The conditions of the gel were: Native Gel (13% Polyacrylamide, 2X MOPS, 10% APS, 2mM Mg^{2+}, TEMED), Loading Buffer (2mM Mg^{2+}, 50 % glycerol, 4X MOPS), Running Buffer (2X MOPS, 2mM Mg^{2+}, H_2O) Reaction Buffer (3 µL/sample: 20mM HEPES pH 7.0, 2mM Mg^{2+}, Sample RNA at [35 µM] and A at [0, 35, 70, 140, 280 µM] using 65SNAP5 annealing protocol) 4 µL sample was added and run at 220 V

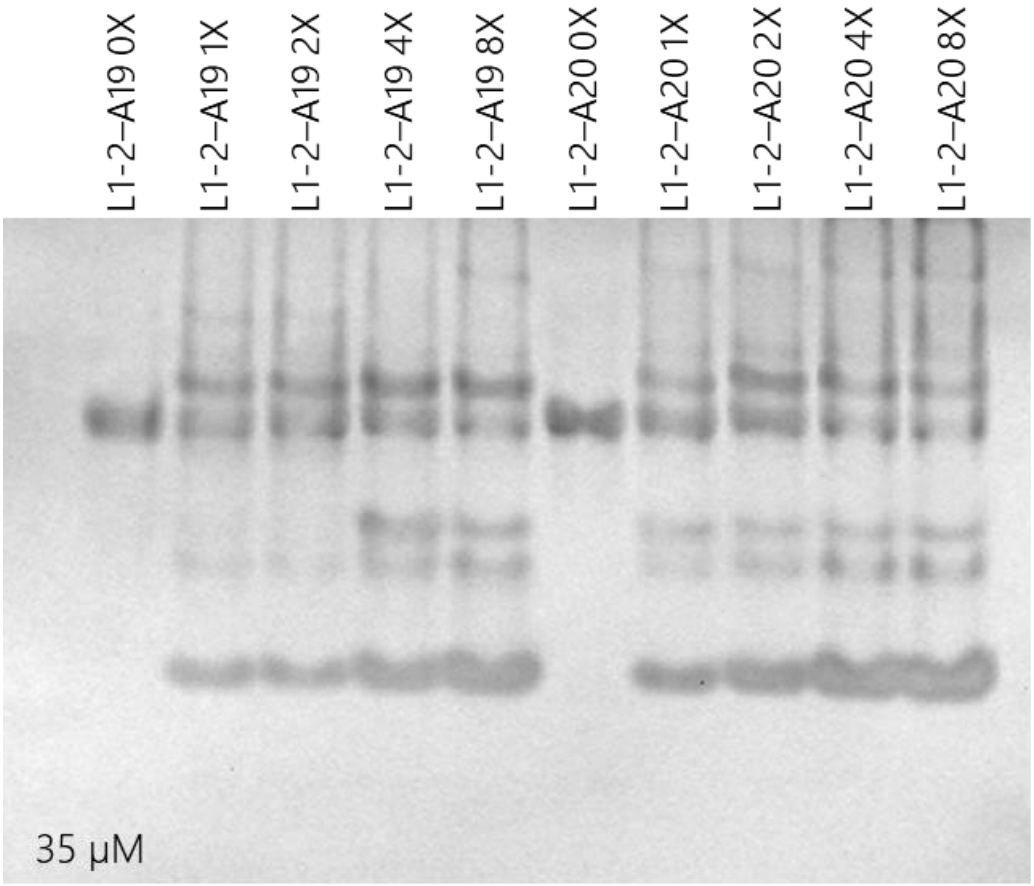

Figure 25. ZRP1-4/2-4 + A19/A20. This gel shows better separation between the larger construct (L1-2) and the complex (L1-2-Ax). The conditions of the gel were: Native Gel (13% Polyacrylamide, 2X MOPS, 10% APS, 2mM Mg^{2+}, TEMED), Loading Buffer (2mM Mg^{2+}, 50 % glycerol, 4X MOPS), Running Buffer (2X MOPS, 2mM Mg^{2+}, H_2O) Reaction Buffer (3 µL/sample: 20mM HEPES pH 7.0, 2mM Mg^{2+}, Sample RNA at [35 µM] and A at [0, 35, 70, 140, 280 µM] using 65SNAP5 annealing protocol) 4 µL sample was added and run at 220 V

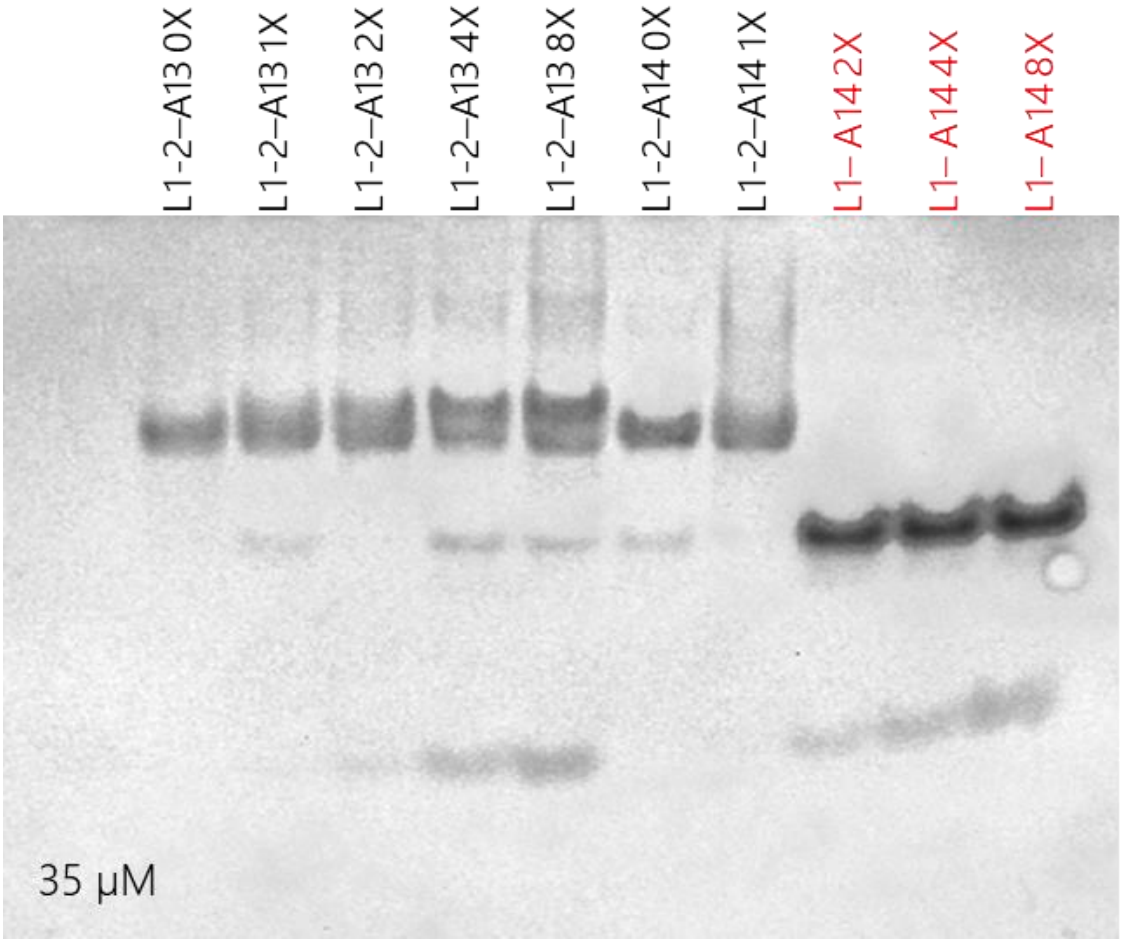

Figure 26. ZRP1-4/2-4 + A413/A14. This gel shows that no complex is formed with either A13 or A14. Additionally, the lanes labeled in red indicates that ZRP2-4 was inadvertently missing. The conditions of the gel were: Native Gel (13% Polyacrylamide, 2X MOPS, 10% APS, 2mM Mg^{2+}, TEMED), Loading Buffer (2mM Mg^{2+}, 50 % glycerol, 4X MOPS), Running Buffer (2X MOPS, 2mM Mg^{2+}, H_2O) Reaction Buffer (3 µL/sample: 20mM HEPES pH 7.0, 2mM Mg^{2+}, Sample RNA at [35 µM] and A at [0, 35, 70, 140, 280 µM] using 65SNAP5 annealing protocol) 4 µL sample was added and run at 220 V

In **Figure 23 and 26 w**e saw only smears indicating that the ternary complex was not forming. In **Figure 24,** we were starting to see some separation, indicating that perhaps antisense DNA length of 17 to 18 nucleotides is the point where we are starting to form the complex. However, in **Figure 25,** we can see the complex forming. Based on those results we concluded

that longer DNA oligos needed also to be tested with the larger construct ZRP1-4 and ZRP2-4 in future experiments.

In vitro transcription

Production of SLA RNA for crystallization was established by *in vitro* transcription. Therefore, we designed a double stranded DNA sequence that can be directly cloned into a vector or can be used directly as a template for *in vitro* transcription. The sequence elements for the DNA insert were the following: Random sequence + EcoRI restriction site + T7 Promoter + ZIKV SLA + XmaI restrction site with a total of 130 bp as shown in **Table 4**.

Table 4. DNA sequence for cloning of the SLA expression vector

G-Block Sequence	
Name	Sequence
ZV-1	5'TACCCGGGTTGAGTTAGTGTTGAGCTCACGGAACGAATTCTAATACGACTCACTATAGGGTTGATCTGTGTGAATCAGACTGCGACAGTTCGAGTTTGAAGCGAAAGCTAGCAACAGTATCAACCCCGGG3'

I cloned the SLA DNA into the pJET 1.2 plasmid from ThermoFisher by using a high-efficiency cloning kit in which blunt or sticky-end DNA donor fragments can be cloned (**Figure 27**). Cloning was successful, and the sequence of the product plasmid was confirmed using pJET F primer (**Table 5**).

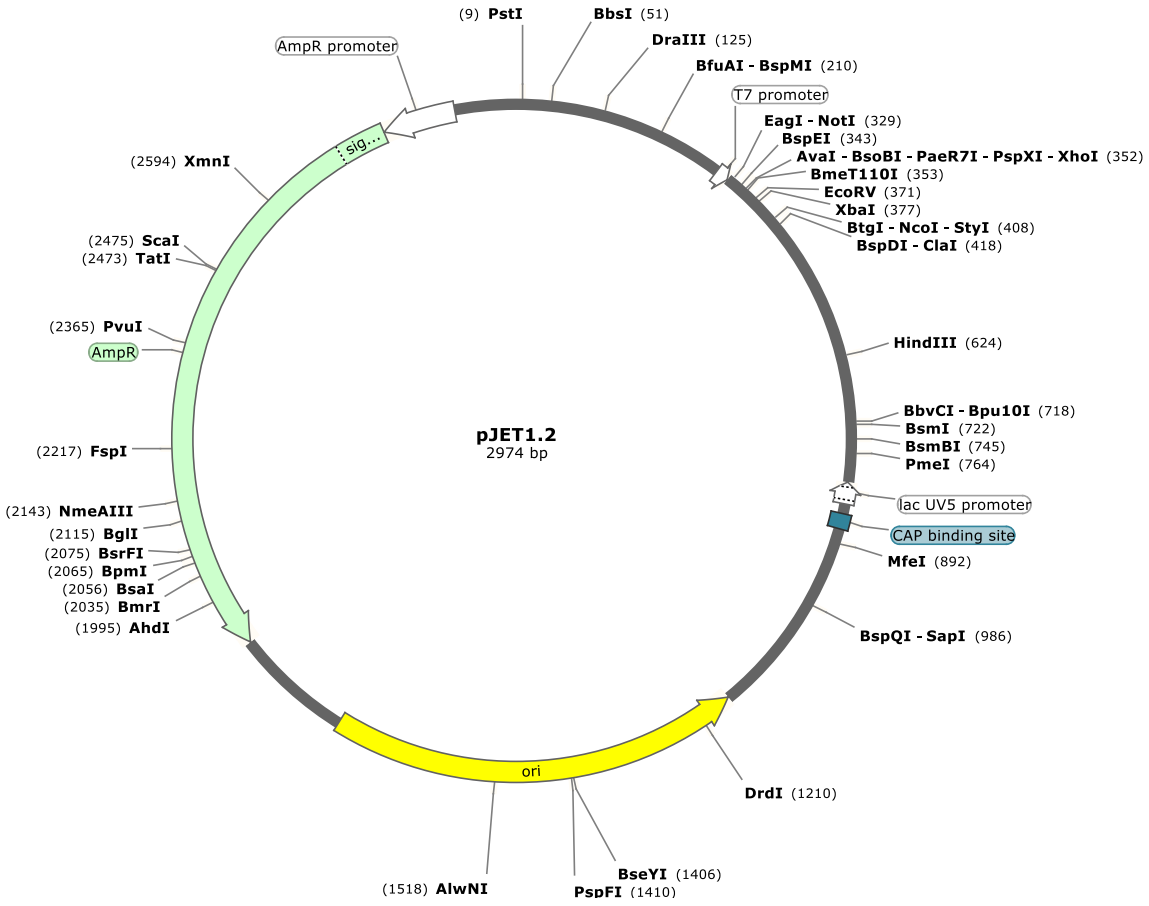

Figure 27. pJET1.2 plasmid map. This figure shows the components of the pJET1.2 plasmid and restriction sites.

Table 5. pJET 1.2 F primer

Primer pJET 1.2	
Name	Sequence
pJET F	5'-CGACTCACTATAGGGAGAGCGGC-3'

After that, the cloned plasmid was used to transform E. coli competent cells (GC10^{TM} Competent Cells-High Efficiency Cat. No. 42-658). The plasmid sequence was again verified, and the plasmid was purified and used for *in vitro* transcription. *In vitro* transcription was performed

using the MEGAscript™ T7 Transcription Kit from ThermoFisher. This kit produces high yield transcripts where the only optimizations needed are an adjustment of the reaction time, and concentration of DNA template concentration and RNA polymerase. In the first *in vitro* transcription, we compared 8h, 12h and 24 h transcription times and observed that 24 h yielded more product in comparison to the shorter times, as shown below:

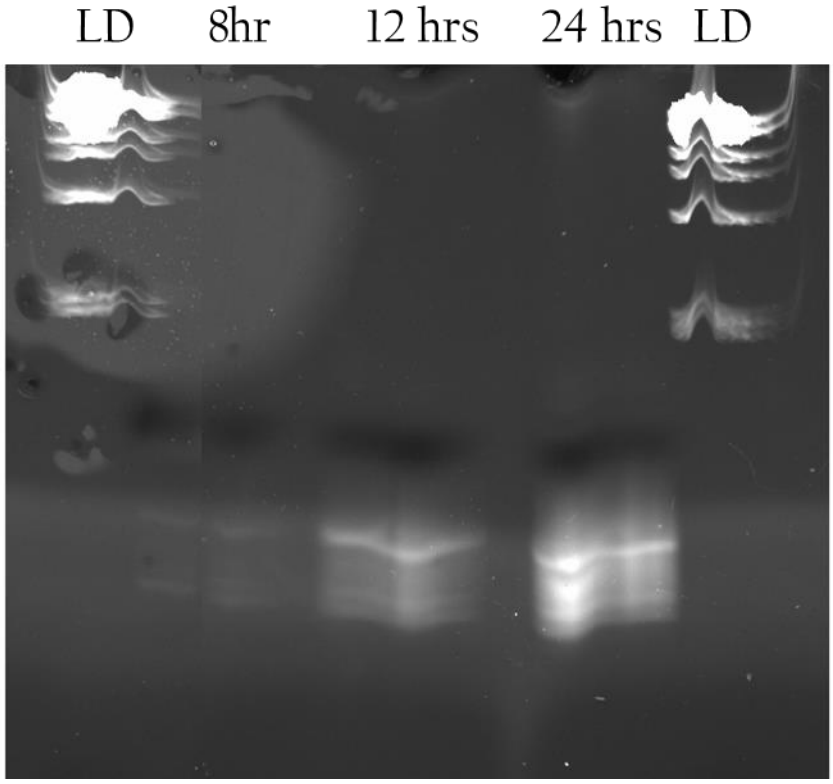

Figure 28. IVT1. This figure shows the amount of SLA RNA transcript obtained after 12 h. and 24 h.

After that, we wanted to test if the amount of enzyme made a difference for the transcription yield. Therefore we tested 1X versus 2X fold enzyme rekative to the recommended amount:

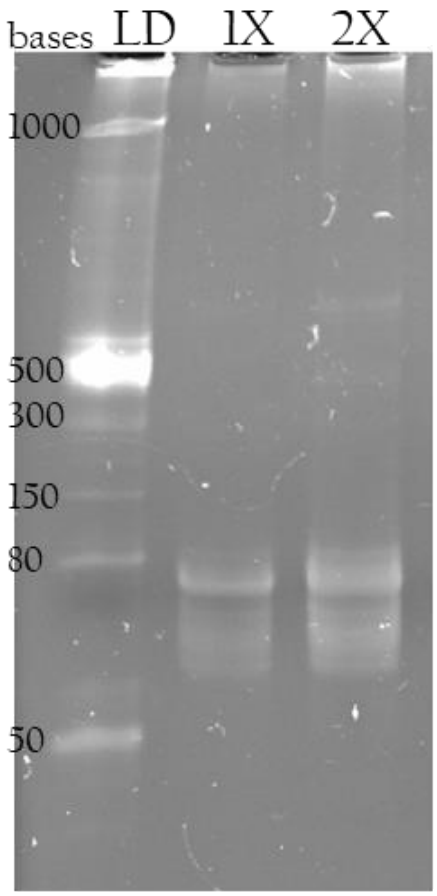

Figure 29. IVT-2 This gel shows the difference in product yield obtained after 24 h with 1X versus 2X the enzyme (from recommended amount), where 2X gave the highest yield. The band on the 2X is twice as intense, indicating more RNA product transcribed compared to 1X enzyme concentration.

In **Figure 28,** we observed that 2-fold enzyme yielded more product; however, we wanted to test the difference between adding 2X the enzyme at the beginning of the reaction compared with 1X the enzyme at the beginning of the reaction and again 12 h later. The result was the same and no noticeable difference in the amount of transcription was observed (results not shown).

The next optimization involved analyzing whether increasing the Mg^{2+} concentration would increase the yield of the transcription. We tested 0, 2, 5 and 10 mM Mg^{2+} and observed that 2, 5, and 10 mM gave more product in comparison to 0 mM Mg^{2+}:

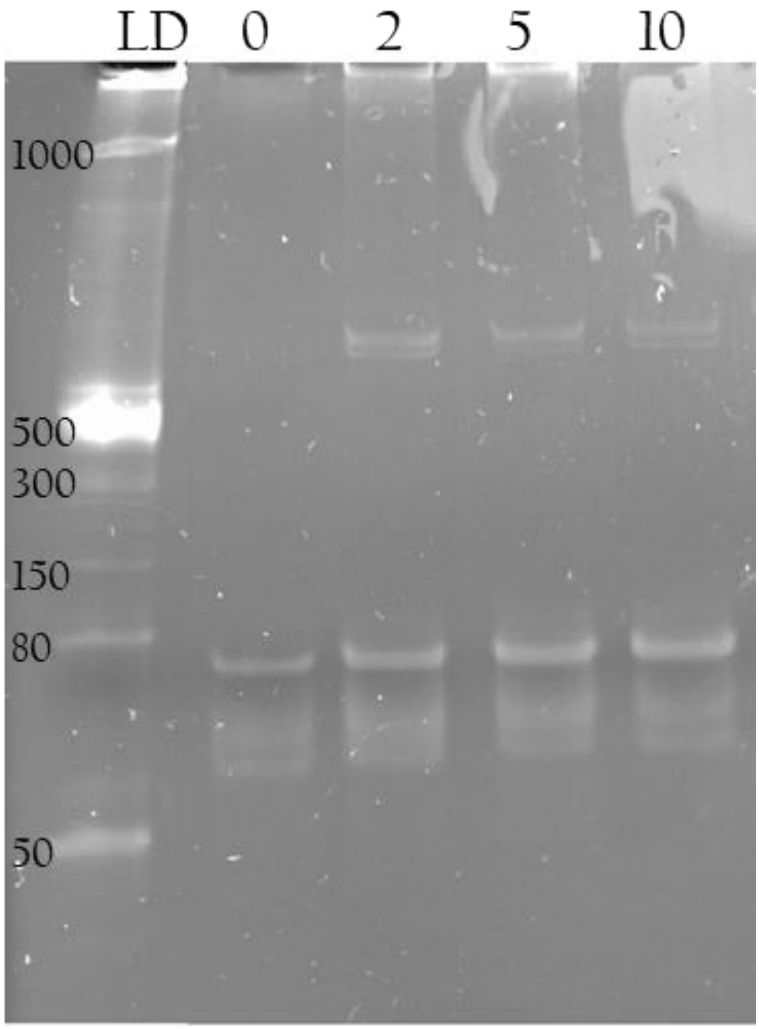

Figure 30. IVT-4. This gel shows the difference in product obtained after 24 h transcription with 2X enzyme and 0, 2, 5 and 10 mM Mg^{2+}. Concentrations of 2, 5, and 10 mg Mg^{2+} resulted in higher yield. The bands at 2, 5, and 10 mM Mg^{2+} were almost twice as intense compared to 0 Mg^{2+}. However, there was no difference between 2, 5 and 10 mM Mg^{2+} Therefore 2 mM Mg^{2+} was selected for the optimized protocol.

The final conditions chosen for the optimized *in vitro* transcription for the ZIKV SLA RNA were: 24 h reaction time, 2X RNA polymerase and 2 mM Mg^{2+}. Subsequently, we increased the reaction volume from 20 µL to 200 µL with 0 and 2 mM Mg^{2+}:

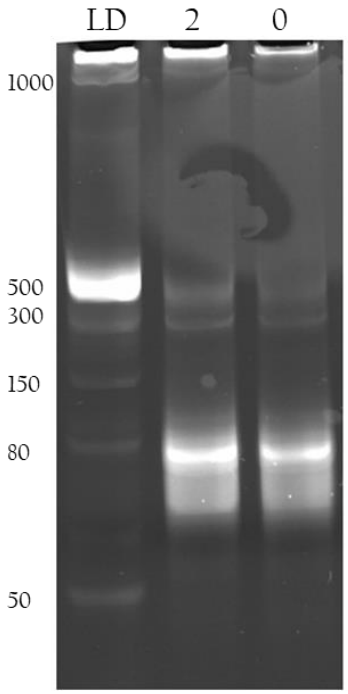

Figure 31. IVT-5. This gel demonstrates a successful 200 µL reaction in which we tested 0, and 2 mM Mg^{2+}. 2 mM Mg^{2+} gave more transcription product.

Figure 31, demonstrated a successful large-scale reaction. The following step was to purify the transcription using PAGE gels, and then use the purified product for crystallization trials.

Crystallography

We first tried to crystallize SLA RNA at 150 µM concentration by hanging-drop vapor diffusion and using a commercially available screening kit (Natrix kit 1 and 2) which tests 48 different buffer, salt and precipitant conditions. Since precipitation was not observed in any of the conditions tested at the initial RNA concentration, we increased the concentration of SLA RNA to 300 µM when we started to observe some precipitation or phase separation. To ensure integrity of the RNA, the transcribed RNA was tested for degradation by gel analysis:

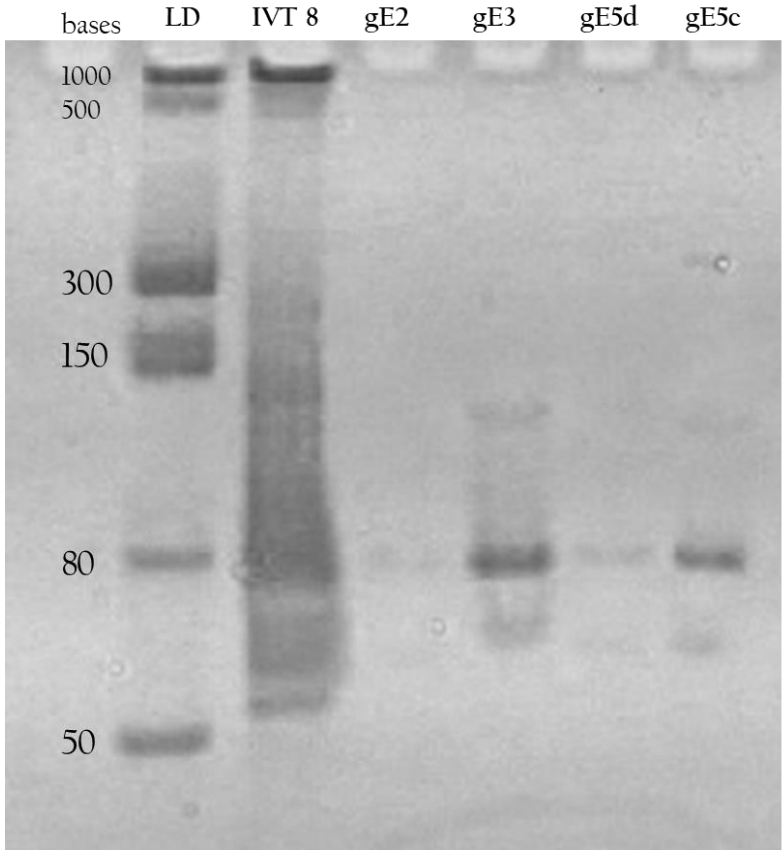

Figure 32. RNA gel analysis. In this gel we used IV8 as our control (unpurified *in vitro* transcription) and we tested RNA extracted from gel purification. Samples gE2 and gE3 contained 1 µL of each purification, 1 µL of loading dye and 8 µL of H_2O. Samples gE5d (diluted) and gE5c (concentrated) contained 0.5 µL of purified sample, 0.5 µL of loading dye and 9 µL of H_2O [gE2] 85 µM, [gE3] 480 µM, [gE5d] 300 µM and [gE5c] 1000 µM

In **Figure 32,** we compared one of the unpurified *in vitro* transcriptions with the gel purifications. Since we obtained single bands for the RNA from gel extraction, we confirmed that there was no degradation of RNA.

Based on the previous results, we decided to increase the RNA concentration for crystallization once more to 900 µM and this time we saw more conditions with some precipitations. While initially no crystals were observed, optimization will continue starting from these conditions.

DISCUSSION

FRET assay

The results of this assay demonstrated that ZIKV SLA is a three-way junction and that the P2 and P3 helical arms are coaxially stacked. Additionally, it was established that 2 mM Mg^{2+} is needed for the folding of the SLA construct and that the three-way junction can be targeted with small molecule ligands. A shorter RNA construct formed a complex with antisense DNA oligomers of 15-17 nt. Consistently, a longer SLA construct formed ternary complex with antisense DNA of 19- 20 nt length.

In Vitro Transcription

DNA templates for the SLA domain in Zika virus were successfully generated for the preparation of RNA by *in vitro* transcription. The sequence of the template was confirmed through sequencing. Optimized conditions for in vitro transcription were chosen based on the transcription efficiency. The best conditions for optimization of 1 µg of linearized plasmid include overnight incubation (24 h) at 37 °C, 2 mM Mg^{2+} and twice the amount of RNA polymerase. The same conditions for the large scale gave positive results, with a high transcription yield.

Crystallography

As mentioned before, well diffracting crystals of the SLA domain will be valuable for structure determination of the RNA target. While whe have not been able to obtain crystals in the initial crystallization trials, we will continue to screen conditions for crystallization.

Future Directions

Milligram quantitie of SLA RNA were obtained, and *in vitro* transcription was optimized producing a good yield in larger scales, enabling future optimization of the crystallization of the ZIKV SLA domain.

Moreover, since it has been shown that flavivirus genome cyclization is essential for viral replication, and that two conformations exist dynamically, the linear and circular conformations, crystal structures will help us understand the function of alternative RNA structures formed in different stages of the viral life cycle.

Finally, the FRET constructs developed in this work can be used to screen for small molecule ligands of the SLA RNA, which will be tested for activity as inhibitors of ZIKV replication.

MATERIALS AND METHODS

FRET

Each 120 µL reaction contained the following depending on the purpose of the experiment:

Testing Mg^{2+} concentration:

ZRP1 and ZRP2 were both at 0.1 µM, Mg^{2+} concentration of (0, 0.2, 2 and 20 mM), DNA oligo at .1 µM, 20 mM HEPES buffer pH 7.0 to 120 µL.

Testing best DNA oligo:

ZRP1 and ZRP2 were both at 0.1 µM, Mg^{2+} concentration of 2 mM, DNA oligo concentrations: 0, 0.1, 0.2, 0.4, 0.8 and 1.6 µM, 20 mM HEPES buffer pH 7.0 to 120 µL.

Testing for antibiotic

ZRP1 and ZRP2 were both at 0.1 µM, Mg^{2+} concentration of (0, 0.2, 2 and 20 mM), Antibiotic concentrations: 0, 0.1, 0.2, 0.4, 0.8 and 1.6 µM, 20 mM HEPES buffer pH 7.0 to 120 µL.

The components were mixed on PCR strips and transferred to the thermocycler, where the selected protocol was used:

65SNAP5: 65 °C for 5 min and snap cool at 4 °C for 5 min

37C30 → 10RT: 37 °C for 30 min followed by RT for 10 min

65SNAP5 + 37C30 → 10RT: 65 °C for 5 min and snap cool at 4 °C for 5 min + 37 °C for 30 min followed by RT for 10 min

65SNAP20: 65 °C for 5 min and snap cool at 4 °C for 5 min + 37 °C for 10 min, RT (22 °C) for at least 2 min or until the enter button was pressed to end the program.

After that, the strips were removed from thermocycler AD 110 µL were transferred to: PP-Microplate, Black, 96 Well, F-Shape, 10 PCS/BAG, REF: 655209, Lot: E130505J, From: Greiner Bio-One, Raw Material Batch: 0109760501. The 96 well plate was placed in the SpectraMax Gemini XS and the following wavelengths were read:

a. Excitation: 520 ; Emission: 570 ; Cutoff: 550

b. Excitation: 520 ; Emission: 670 ; Cutoff: 550

c. Excitation: 520 ; Emission: 670 ; Cutoff: 665

d. Excitation: 620 ; Emission: 670 ; Cutoff: 665

Native gel

All Native gels were 13% acrylamide, containing ammonium persulfate (APS), 2 mM Mg^{2+} and TEMED. Running buffer contained MOPS, 2 mM Mg^{2+} and H_2O, the reaction buffer contained HEPES pH 7.0, RNA, and varying amounts of Mg^{2+}, or DNA oligos. The loading buffer contained 2 mM Mg^{2+}, 50% glycerol and 4X MOPS. The gels were ran at 20V/cm

Agarose Gel Electrophoresis

1% agarose gels agarose were made using 1XTAE. The solution was microwaved for 1-3 min until agarose was completely dissolved, then cooled down until it was comfortable to touch, ethidium bromide (EtBr) was added to a final concentration of approximately 0.2-0.5 µg/mL. The agarose solution was poured into gel tray, the comb was added and it sat at RT until it was fully polymerized. Loading buffer was added to samples as well as a DNA ladder. Gels were run with 1X TAE at 100 V

Cloning

The sequence of interest forming the SLA domain was designed and ordered as a g-block from Integrated DNA Technology (IDT) (**Table 7**). The g-block was resuspended to a concentration of 10 ng/µL and inserted into the pJET1.2/blunt vector from ThermoFisher Scientific #K1231. Each 10 µL reaction contained 25 ng pJET1.2/blunt Cloning Vector, 1x Reaction Buffer, 10 ng of g-block, 2.5 U of T4 DNA ligase AD water. Reactions were slightly vortexed and centrifuged for 3-5 seconds, then incubated at RT for 10 min, on ice for 2 min, followed by transformation of E. coli.

Transformation of E. coli

50 µL of E. coli competent cells (GC10^{TM} Competent Cells-High Efficiency Cat. No. 42-658) were thawed; 5 µL of the ligated solution was gently added and incubated in ice for 30 min, followed by heat shock at 42 °C for 45 sec then incubated at in ice for 2 min. SOC stock at 37 °C was added to the competent cells and was incubated in the shaker for 1 hr and then plated in a Amp plate. Plate was incubated at 37 °C for 12-18 hrs.

Plasmid DNA purification

To isolate the plasmid, a colony forming unit from the Amp plates of the transformed E. coli was grown in 3 ml LB media containing 50 µg/ml ampicillin at 37 °C overnight. The plasmid was purified using The Wizard® *Plus* SV Minipreps DNA Purification System Cat. A1330 from Promega. Purification was performed according manufacturer's recommendations and 60 ng/µL

were sent to ETON for sequencing, using primers contained in the pJET cloning kit (**Table 8**). Glycerol stocks were made from colonies confirmed with sequencing.

Restriction Digest and Vector Linearization

The plasmid was digested and dephosphorylated in a 50 µL reaction containing: 1x CutSmart buffer (NEB), 1 µg of plasmid, 20 U XmaI-HF (NEB) 5 U Alkaline Phosphatase, Calf Intestinal (CIP) (NEB) and H_2O. The reaction was incubated at 37 °C for 45 min the heat inactivated for 20 min. Digestion was terminated using 1/20 volume of 0.5 M EDTA pH 8.0, 1/10 volume of 3M Na acetate and 2 volumes of ethanol. The solution was mixed and incubated at -20 °C for at least 15 min. The solution was centrifuged at top speed (14k RPM) for 15 min and the supernatant was removed. The pellet was resuspended in 10 µL of TE buffer.

***In vitro* transcription**

Small *in vitro* transcription reactions were done in a 20 µL volume and larger scale reactions were done in 200 µL volume using the T7 MEGAscript® Kit from ThermoFisher following the manufacture's recommendations. Each small reaction contained 7.5 mM of each ATP, CTP, GTP, and UTP solution, 1 µg of digested plasmid,1x reaction buffer, 2x T7 Enzyme mix AD 2 mM Mg^{2+}; the solution was mixed gently and incubated at 37 °C for 24 hrs. After incubation, 2 U of Turbo DNase mix was added and incubated again at 37 °C for 15 min.

Phenol/Chloroform extraction

For the small transcription reactions, 115µL Nuclease-free Water and 15µL Ammonium Acetate Stop Solution was added and mixed thoroughly, equal volume of phenol: chloroform isoamyl alcohol 25:24:1 (v/v) was added and vortexed for 20 seconds, centrifuged at RT for 5 min and the aqueous solution was transferred to a new microcentrifuge tube. The RNA was precipitated by adding 1 volume of 100 % isopropanol mixing well. The solution was incubated for at least 15min at –20°C. Centrifuged at 4°C for 15min at maximum speed to pellet the RNA. The supernatant was removed and the RNA was resuspended in H_2O and stored at -20 °C.

Denaturing Urea-Polyacrylamide Gel Electrophoresis

Gels were either 13% or 15 % acrylamide-8 M Urea. Gels were prepared using urea, acrylamide, TBE, ammonium persulfate (APS), and TEMED. RiboRuler Low Molecular Range ssRNA Ladder (NEB) used in the first lane per manufacturer's recommendation. Each lane contained 3 µL of the transcription reaction and 1x Gel Loading Buffer II (from MEGAscript® Kit). Samples were heated to 65˚C for 3-5 minutes before loading on the gel. Gels were run at 20 V/cm with a maximum current of 25 mA. Gels were stained for 10 minutes in 5 µg/mL ethidium bromide (EtBr) and visualized using a Multi Doc-It Digital Imaging System 2UV Transilluminator (UVP) at 302 nm. For large-scale transcription, UV shadowing using 254 nm radiation from a handheld lamp and a TLC plate to visualize the RNA without staining.

RNA Purification

Relevant bands were cut directly from the gel using a clean razor blade. The gel was crushed by forcing the gel through a small syringe. The gel pieces were placed into a 1.5 ml micro centrifuge tube with enough TEN buffer to cover the gel pieces. The gel was eluted on a rotary shaker overnight at 4˚C. The tube was spun to pellet the gel fragments. The supernatant was passed through a 0.2 µM filter into a new centrifuge tube. The RNA was recovered by the addition of 3 volumes of ethanol and incubated overnight at -20 °C. the tube was centrifuged and the pelleted RNA was resuspended in 1 mL of 1M sodium cacodylate pH 6.5. the RNA was transferred into a Centricon concentrator. The RNA was concentrated to about 290 µL and more 1 M sodium cacodylate pH 6.5 was added to desired concentration. For crystallography we tried 150 µM, 300 µM and up to 900 µM RNA

REFERENCES

[1] Abe N, Matsumoto K, Nishihara M, Nakano Y, Shibata A, Maruyama H, Shuto S, Matsuda A, Yoshida M, Ito Y, Abe H. Rolling Circle Translation of Circular RNA in Living Human Cells. Scientific Reports. 2015:16435.

[2] Alekhina OM, Vassilenko KS. Translation initiation in eukaryotes: versatility of the scanning model. Biochemistry (Moscow). 2012;77:1465-77

[3] Beckert, B., & Masquida, B. (n.d.). Chapter 3 Synthesis of RNA by In Vitro Transcription. https://doi.org/10.1007/978-1-59745-248-9

[4] Boerneke, M. A., Dibrov, S. M., Gu, J., Wyles, D. L., & Hermann, T. (2014). Functional conservation despite structural divergence in ligand-responsive RNA switches, 111(45). https://doi.org/10.1073/pnas.1414678111

[5] Boerneke, M. A., & Hermann, T. (2015). Conformational flexibility of viral RNA switches studied by FRET, 91, 35–39. http://doi.org/10.1016/j.ymeth.2015.09.013

[6] Caplinger, Christopher. "Yellow Fever Epidemics." *Yellow Fever Epidemics | Entries | Tennessee Encyclopedia*, 25 Dec. 2009, tennesseeencyclopedia.net/entry.php?rec=1545.

[7] Deforges J, Locker N, Sargueil B. mRNAs that specifically interact with eukaryotic ribosomal subunits. Biochimie. 2015.

[8] Eden VM, Byrd MP, Sherrill KW, Lloyd RE. Demonstrating internal ribosome entry sites in eukaryotic mRNAs using stringent RNA test procedures. Rna. 2004.

[9] Fluorescence Resonance Energy Transfer (FRET)-Note 1.2. (n.d.). R, from https://www.thermofisher.com/sa/en/home/references/molecular-probes-the-handbook/technical-notes-and-product-highlights/fluorescence-resonance-energy-transfer-fret.html

[10] Fraser CS, Doudna JA. Structural and mechanistic insights into hepatitis C viral translation initiation. Nat Rev Micro. 2007;5:29-38.

[11] Gallo S, Furler M, Sigel R. In vitro Transcription and Purification of RNAs of Different Size. CHIMIA International Journal for Chemistry. 2005;59:812.

[12] Gebhard, L. G., Filomatori, C. V., & Gamarnik, A. V. (2011). Functional RNA elements in the dengue virus genome. *Viruses*, *3*(9), 1739–1756. https://doi.org/10.3390/v3091739

[13] Golden, B. L. (n.d.). Preparation and Crystallization of RNA.

[14] Hinnebusch AG. Molecular mechanism of scanning and start codon selection in eukaryotes. Microbiology and Molecular Biology Reviews. 2011.

[15] History.com Staff. "First Victim of Memphis Yellow-Fever Epidemic Dies." *History.com*, A&E Television Networks, 2009, www.history.com/this-day-in-history/first-victim-of-memphis-yellow-fever-epidemic-dies.

[16] Holbrook, S. R., Kim, S., National, L. B., & Building, M. C. (1997). RNA Crystallography, 98.

[17] Jackson RJ, Hellen CUT, Pestova TV. The mechanism of eukaryotic translation initiation and principles of its regulation. Nature reviews Molecular cell …. 2010.

[18] Kieft, J. S. (2009). Viral IRES RNA structures and ribosome interactions, 33(6), 274–283. https://doi.org/10.1016/j.tibs.2008.04.007.Viral

[19] Kuno, G., Chang, G. J., Tsuchiya, K. R., Karabatsos, N., & Cropp, C. B. (1998). Phylogeny of the Genus Flavivirus, 72(1), 73–83.

[20] Martinez-Salas E, Pacheco A. New insights into internal ribosome entry site elements relevant for viral gene expression. Journal of General Virology. 2008.

[21] Martínez-Salas E, Piñeiro D. Alternative mechanisms to initiate translation in eukaryotic mRNAs. Comparative and Functional Genomics 2012.

[22] Modes of energy transfer between fluorophores and quenchers. Marras Laboratory, Public Health Research Institute, www.molecular-beacons.org/toto/Marras_energy_transfer.html.

[23] Pawar, M. G., Nuthanakanti, A., & Srivatsan, S. G. (2013). Heavy Atom Containing Fluorescent Ribonucleoside Analog Probe for the Fluorescence Detection of RNA-Ligand Binding.

[24] Plank TDM, Kieft JS. The structures of nonprotein‐coding RNAs that drive internal ribosome entry site function. Wiley Interdisciplinary Reviews: RNA. 2012.

[25] Schürer H, Lang K, Schuster J, Mörl M. A universal method to produce in vitro transcripts with homogeneous 3′ ends. Nucleic Acids Research. 2002;30.

[26] Sekar RB, Periasamy A. Fluorescence resonance energy transfer (FRET) microscopy imaging of live cell protein localizations. The Journal of Cell Biology. 2003;160(5):629-633. doi:10.1083/jcb.200210140.

[27] Shandrick, S., Zhao, Q., Han, Q., Ayida, B. K., Takahashi, M., Winters, G. C., Hermann, T. (2004). Monitoring Molecular Recognition of the Ribosomal Decoding Site**, 3177–3182. https://doi.org/10.1002/anie.200454217

[28] Sonenberg N, Hinnebusch AG. Regulation of translation initiation in eukaryotes: mechanisms and biological targets. Cell. 2009;136:731-45.

[29] Svitkin YV, Siddiqui N, Sonenberg N. Protein Synthesis Initiation in Eukaryotes: IRES-mediated Internal Initiation. eLS: John Wiley & Sons, Ltd; 2001.

[30] Sztuba-Solinska, J & Le Grice, S. F. Insights into Secondary and Tertiary Interactions of Dengue Virus RNA by SHAPE https://doi.org/10.1007/978-1-4939-6412-3

[31] "Viral Hemorrhagic Fevers (VHFs)." *Centers for Disease Control and Prevention*, Centers for Disease Control and Prevention, 1 Apr. 2014, www.cdc.gov/vhf/virus-families/flaviviridae.htm

[32] Walsh, D., & Mohr, I. (2011). Viral subversion of the host protein synthesis machinery. Nature Publishing Group, 9(12), 860–875. https://doi.org/10.1038/nrmicro2655

[33] Westhof, E. (2006). Topology of three-way junctions in folded RNAs, 83–93. https://doi.org/10.1261/rna.2208106.In

[34] Woodson, S. A., & Koculi, E. (2009). Analysis of RNA Folding by Native Polyacrylamide Gel Electrophoresis. Biophysical, Chemical, and Functional Probes of RNA Structure, Interactions and Folding: Part B (1st ed., Vol. 469). Elsevier Inc. https://doi.org/10.1016/S0076-6879(09)69009-1

[35] Zhou, S., Rynearson, K. D., Ding, K., Brunn, N. D., & Hermann, T. (2013). Bioorganic & Medicinal Chemistry Screening for inhibitors of the hepatitis C virus internal ribosome entry site RNA. Bioorganic & Medicinal Chemistry, 21(20), 6139–6144. http://doi.org/10.1016/j.bmc.2013.03.054

[36] "Zika Virus." *Centers for Disease Control and Prevention*, Centers for Disease Control and Prevention, 2 Feb. 2018, www.cdc.gov/zika/index.html.